Spring 2005

Fabrication and Compressive Yield Strength of Open Cell Corrugated Cellular Solids

Jeong Ho Choi
Embry-Riddle Aeronautical University - Daytona Beach

Fabrication and Compressive Yield Strength of Open Cell Corrugated Cellular Solids

By

Jeong Ho Choi

A Thesis Submitted to the Aerospace Engineering Department in Partial Fulfillment of the Requirements for The Degree of Master of Science in Aerospace Engineering

Embry Riddle Aeronautical University
College of Engineering
Daytona Beach, Florida
Spring 2005

Fabrication and Compressive Yield Strength of
Open Cell Corrugated Cellular Solids

By

Jeong Ho Choi

This thesis was prepared under the direction of the candidate's thesis committee chairman, Dr. David J. Sypeck, Department of Aerospace Engineering, and has been approved by the members of his thesis committee. It was submitted to the Office of the Graduates Programs and was accepted in partial fulfillment of the requirements for the degree of Master of Science in Aerospace Engineering.

THESIS COMMITTEE

David J Sypeck .
Dr. David J. Sypeck
Chairman

.
Dr. Yi Zhao
Member

Frank Radosta .
Dr. Frank Radosta
Member

L. L Narayanaswami .
MSAE Graduate Program Coordinator

. 5/3/2005
Department Chairman, Aerospace Engineering Date

ACKNOWLEDGEMENTS

I would like to extend my appreciation Dr. David J.Sypeck for his guidance and advice, as well as Dr. Frank Radosta and Dr. Yi Zhao for their assistance and advice. Finally, I would like to extend my deepest gratitude and appreciation to my wife Young Mi for her love and support. Also, thanks to my friend Jeff Schneider for his help.

ABSTRACT

Author: Jeong ho Choi

Title: Fabrication and Compressive Yield Strength of Open Cell Corrugated Cellular Solids

Institution: Embry-Riddle Aeronautical University

Degree: Master of Science in Aerospace Engineering

Year: 2005

This thesis studied the fabrication and compressive yield strength of open cell corrugated cellular solids made from type 304 stainless steel. Test samples were made by corrugating woven wire meshes, then laminating these in a high temperature argon environment. Mesh sizes ranging from 9.5 pore/cm (24 pore/in) to 31.5 pore/cm (80 pore/in) with wire diameters ranging from 0.178 mm (0.007 in) to 0.3556 mm (0.014 in) were bonded using lithobraze 925 (Ag-7.5Cu-0.2Li) to create cellular solids having relative densities ranging from 0.0384 to 0.0920. Test samples were then quasistatically compressed to measure the stress-strain response. The stress level at 25% strain (compressive yield strength) was plotted as a function of relative density and then compared to predicted behavior. It was found that the relative compressive yield strength variation with relative density could be accurately modeled using the Gibson-Ashby open cell model.

TABLE OF CONTENTS

LIST OF TABLES

LIST OF FIGURES

1. INTRODUCTION

1.1 Cellular Solids

The term cellular is defined as "relating to, resembling, consisting of or containing a cell or cells". In nature, cells are often found within plant and animal tissue [1]. The term solid on the other hand, suggests substances having a definite shape and volume: one that is neither liquid nor gaseous.

Cellular solids are made up of interconnected networks of solid struts or plates that form the edges and faces of cells [2]. Many materials have a cellular structure: an assembly of prismatic or polyhedral cells with solid edges and faces packed together to fill space [3]. Natural cellular materials include cork, balsa wood, sponges, trabecular bones, cancellous bones (see Fig. 1-1), etc. Food items with cellular architectures include bread, meringue, chocolate bar, junk food crisp, malteser, jaffa cake, etc [2]. Fibrous cellular solids include felt, paper, cotton, wool, and the heat resistant tiles on the Space Shuttle [2]. Cellular bubble mat materials include soap bubbles, honeycombs, bubble rafts, and hollow sintered aluminum spheres [2]. Synthetic honeycombs (see Fig. 1-2) and synthetic stochastic foams (see Figs. 1-3 and 1-4) are made from polymers, metals, ceramics, and glasses, and fall into the category of engineered cellular materials [3]. The cellular solids described above generally exhibit open, closed or a mixed type of porosity and a large diversity exists.

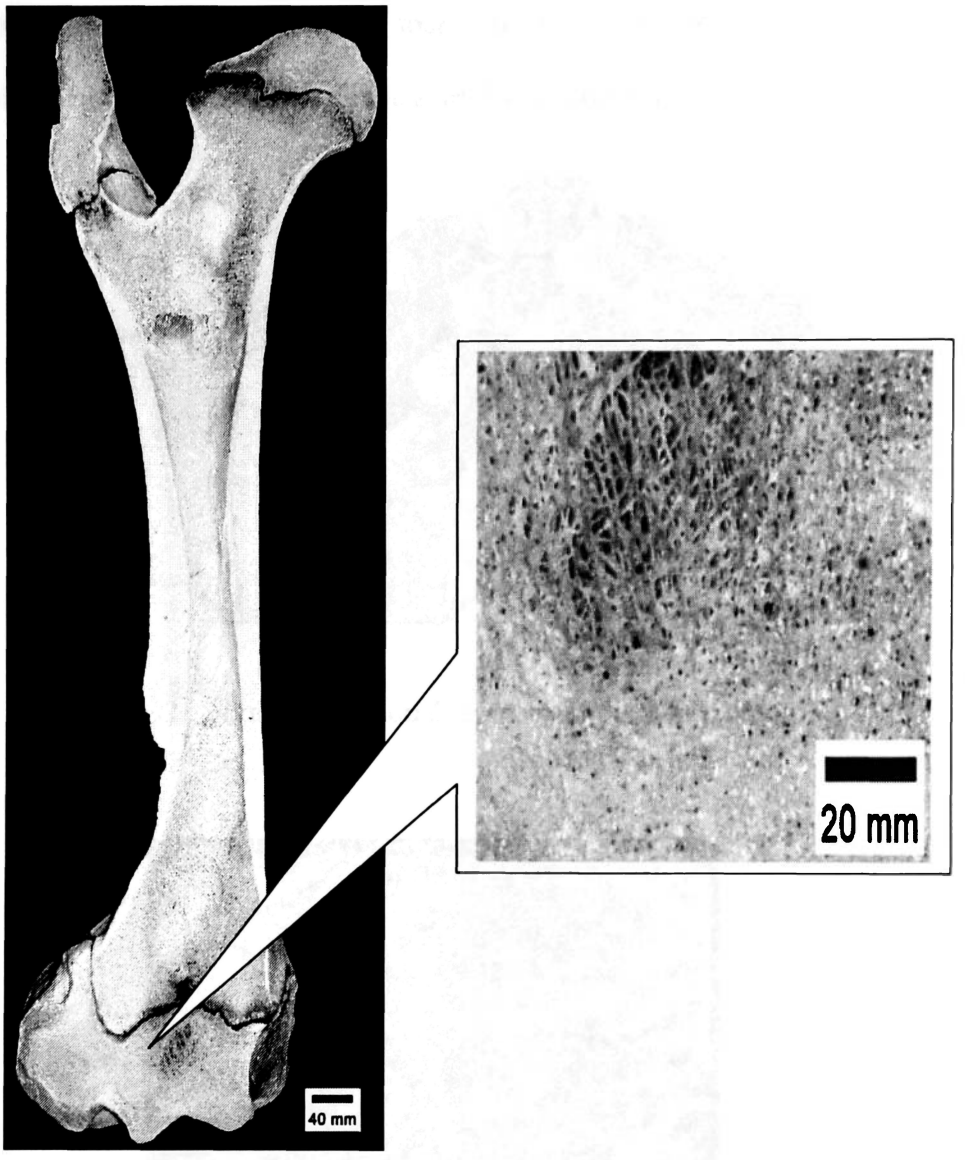

Figure 1-1. Bovine femur and expanded view of the cancellous bone core.

Many biological materials have evolved into a cellular construction since cellular architectures offer the possibility to improve properties such as stiffness, density, and strength according to environmental conditions [4]. The cell structures of most engineered cellular solids have evolved based upon those of natural cellular solids.

Successful examples of open or closed cell foams include foam seat cushions (closed cell polymer foams), honeycomb core floor panels, and reticulated open cell foams.

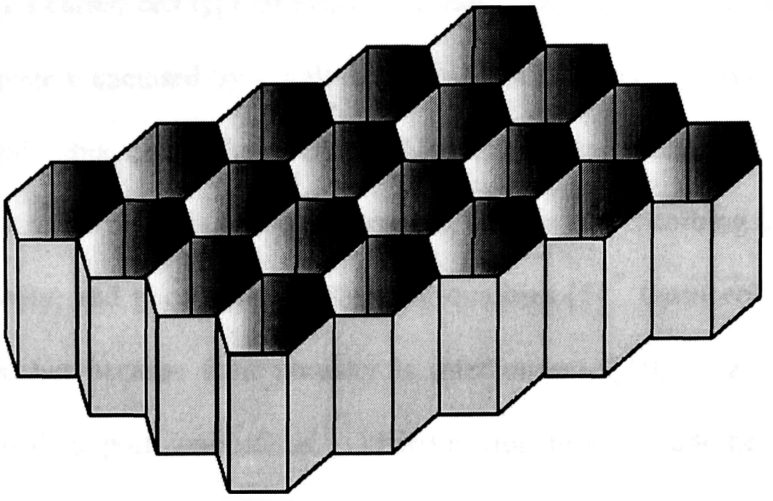

Figure 1-2. Three-dimensional representation of honeycomb.

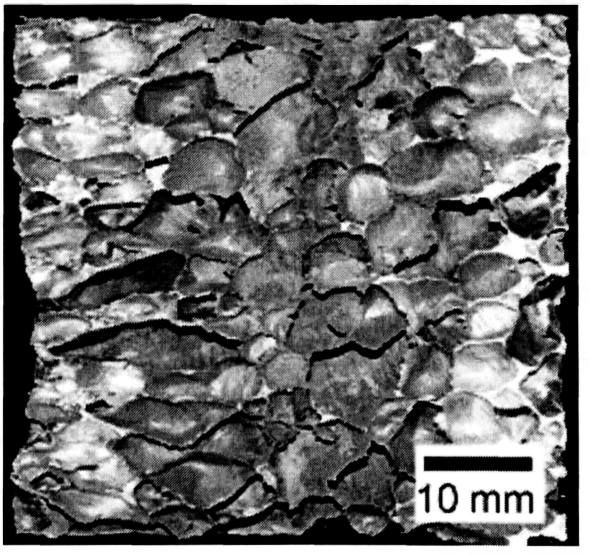

Figure 1-3. Closed cell stochastic aluminum foam (Alcan International Limited, Kingston, Ontario).

Cellular solids can be categorized into three fundamental structures: honeycombs (see Fig. 1-2), open cell stochastic foams (see Fig. 1-4), and closed-cell stochastic foams (see Fig. 1-3). In a closed cell type of foam, each individual cell, more or less spherical in shape, is completely enclosed by a wall of material. In an open cell type of foam, the porosity within individual cells is interconnected, as in a natural sponge [6]. Closed cell metal foams have relatively high modulus, strength, and energy absorbing capacity, low thermal conductivity, and good acoustic damping qualities [5]. Open cell foams have similar attributes, but because their porosity is interconnected, they can be used for multifunctional load support applications. Other functionalities include heat dissipation applications, porosity for bone in-growth, and storage space for chemicals or fuels [5].

For open and closed cell stochastic foams, models describing physical behavior are approximate because the architecture is not uniform or repeatable. Consider that in open cell metal foams, the solid material is contained randomly within cell ligaments and plateau borders. In closed cell structures, on the other hand, where each cell is sealed from its neighbor, the material is also randomly distributed within the cell faces, their intersections, and plateau borders [5]. These issues lead to difficulties in representing the cell architecture in a mathematically tractable form and numerous geometrical simplifications are often made.

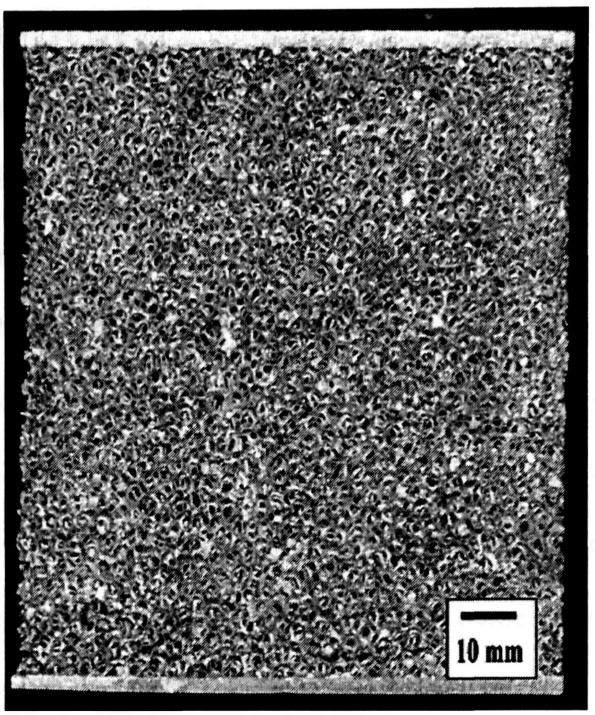

Figure 1-4. Open cell stochastic aluminum foam with aluminum face sheets (Duocel®, ERG Aerospace Inc., Oakland, CA).

One important feature of a cellular solid is its relative density, ρ^*/ρ_s; that is, the density of the cellular material, ρ^*, divided by that of the solid from which the cell walls are made, ρ_s [2]. A second important feature of a cellular solid is its relative compressive yield strength, σ^*/σ_{ys}; that is, the compressive yield strength of the cellular solid, σ^*, divided by the yield strength of the solid from which the cell walls are made, σ_{ys}. A third important feature of a cellular solid is its relative Young's modulus, E^*/E_s; the Young's modulus of the cellular solid, E^*, divided by that of the solid from which the cell walls are made, E_s.

The relative density of some cellular solids (special ultra-low-density foams) may be as low as 0.001. For polymeric foams this can range from 0.05-0.2; for cork it is about

0.14; and for softwoods, 0.15-0.40 [2]. Larger than 0.3, the structure can be treated as a solid containing isolated pores [2]. As the relative density increases, the cell walls thicken and the pore volume fraction decreases.

Cellular solids are very different from aqueous foams (e.g., soap bubbles, soda froth, etc.) because the base materials are solids as opposed to liquids. In many instances, this makes them more difficult to produce. For example, polymeric and metallic foams are usually formed from materials that are significantly more viscous than water and often rely on careful control over composition, processing, temperature, etc. Heat transfer, phase transition, and viscoelastic effects may come into play during their production [7] requiring more effort and control.

1.2 Applications

Cellular solids are currently used for many structural applications [8]. Beams, plates, and reflectors can be made utilizing cellular solids. With numerous cells, there exists structural redundancy such that even if some cells have been punctured (e.g., in the vacuum of space), and loose internal pressure, the damage remains local and does not harm the whole system. Multi-cellular inflatable elements provide redundancy in both general applications as well as high technology aerospace applications. Closed cell plastic foams are used extensively as supports for floating structures and as flotation in boats [9]. Because the field of cellular solids has potential for generating many new forms of cellular solids, especially in the biomedical field, open cell and closed cell foams have also been used for applications involving biological research. Molecular cell biology, enzyme research, immunology, genetic engineering, and implant applications

have all benefited from cellular solids [10-14]. In the aerospace field, stochastic foams find application in commercial aerospace and military applications, the Space Shuttle, various manufacturing industries, etc. [39, 41, 43]. Thus, the structure and properties of cellular solids have fascinated scientists and engineers for centuries [3].

The mechanical properties of cellular solids have been the subject of continuing research and widespread study primarily because of their good weight specific mechanical properties (e.g., high weight specific stiffness and strength comparable to wood). The mechanical properties of cellular solids have led to their use in sophisticated applications in which weight benefit and strength are significant [4, 6, 8]. They also have good energy absorbing [15] and insulating characteristics (resist both sound and heat transmission), like those that occur widely in nature, such as parts of plants, bones, feathers, tissues, etc. [16]. Open cell sponges are attractive as catalyst carriers or as components in heat exchangers [17]. Closed cell foams are used as the core material for lightweight sandwich panels or as crash-absorbers [17]. Synthetic honeycombs have been used extensively as energy absorbers or cushions that resist impact and contact loads from foreign objects [18].

Over the past few years, a variety of metallic and polymeric foams have been produced for a wide range of potential applications such as the cores of sandwich panels and various automotive parts. The typical aim is to develop lightweight structures that are adequately stiff and strong [19]. Foamed plastics have had important uses since primitive man began to use wood, which is a cellular form of the polymer cellulose [20].

The application of cellular foams has mostly been as thermal insulation and its products include disposable coffee cups, booster rocket insulation for the Space Shuttle,

fire protection in modern buildings, refrigerated trucks, railway cars, liquid natural gas ships, etc. [2]. Thermal expansion of materials is of considerable interest since materials in service may experience a considerable range of operating temperatures. For cellular materials, the thermal expansion coefficient is the same as the solid from which it is made [2, 21]. The application field of porous ceramics has recently expanded to thermal and acoustic insulation, kiln furniture, catalyst support, and hot gas, water or molten metal filters [5].

The most noticeable example of cellular solids application is sandwich panels [2]. Sandwich panels are used widely in industry: space vehicles, skis, racing yachts, portable buildings, helmets for head protection, etc. Sandwich plates and shells are structural members consisting of two stiff and strong faces (skins) separated by a lightweight core. Composite sandwich plates and shells are also gaining popularity in engineering practice, due to their high stiffness-to-weight ratio, low thermal conductivity, and energy absorption characteristics [6]. In addition, sandwich composite laminates have also been using widely in aircraft structures to maximize the bending stiffness per unit weight of structural components [18].

Cellular solids have undergone three generations of biomedical material advancement. During the 1960's and 1970's, a first generation of biomedical materials was used inside the human body. A second generation of biomedical materials began to shift the emphasis from achieving exclusively a bio-inert tissue response to producing bioactive components that could elicit a controlled action in the physiological environment. The third generation was designed to stimulate specific cellular responses at the molecular level [11]. Typical cellular materials, such as vertebral trabecular bone,

have been investigated using an analytical cell model comprised of doubly tapered struts. These capture global mechanical properties, while mathematical models for trabecular bone have been developing in order to capture the dominant behavior [10].

Cellular solids have been used extensively in engineering, science, industry, medicine, and so on. The significance of cellular solids has been increasing and is expected to become even more important in the future.

1.3 Previous Research

The structure of cellular solids is thought to have first been scientifically studied during the 1660's when Robert Hooke examined a section of cork in his microscope and first used the term "cell" to describe its structure [3]. Previous studies on the behavior of cellular materials have mainly involved foam materials with randomly shaped and distributed cells [22]. For example, during the late 1970's and early 1980's, the US Army Corps of Engineers researched various forms of cellular solids as a means of improving the structural and functional behavior of soils and aggregate infill materials [23]. Numerous methods for manufacturing cellular polymers, metals, ceramics, glasses and composites with open and closed cell morphologies have been subsequently developed [24].

Many prior scientific studies of cellular materials mainly involved structures with periodic morphogenesis (for example, arrays of tubes and honeycombs) [25]. Cellular metal structures with open cell topologies have been shown as an attractive heat exchange media for a wide range of applications where dissipation of high intensity heat over a relatively compact space is required [26]. It has been more than fifty years since

the method of melt foaming was proposed for preparing foamed aluminum, (which is a closed cell foam with a macroscopic cellular structure). These materials have found use in aerospace, automotive, railway, and other industries [27].

Motivated by recent advances in materials science, manufacturing, and optimization, attention is being focused on metallic sandwich panels for a variety of applications [22]. Advancements in high temperature polymeric materials at NASA Langley have also led to the development of new polyimide foam systems with attractive properties [20]. Computer software for generating simulated foam structures and minimizing their surface energy has made detailed descriptions of the cell structure within a cellular solid possible [3]. Innovative materials laboratories in Japan have developed ultra-lightweight cellular metals with open cells that exhibit extraordinarily high porosities, low apparent densities, and excellent shock absorbency. These are expected to find application as ultra-light cellular metal components in aerospace industries and construction [28].

Modern manufacturing processes have allowed cellular cores to be affordably assembled and bonded to dense face materials, presenting a promising new alternative to the construction of high-performance sandwich panel structures [29]. To help design such structures, previous micro-structural finite element models, which likely started with researchers seeking to investigate the properties of bone (stiffness and tissue stress), were verified for a large number of specimens [10]. The scaffold of bone is often designed as a porous structure (open cell material) with appropriate porosity, pore size, shape and intricate interconnectivity so that a desirable biological network for cell migration, nutrient transportation, and mechanical stiffness and strength can be obtained [30].

The metal textile derived cellular metals are the three-dimensional analogue of metallic textile screen meshes which have already been extensively used in fields such as aerospace, chemical production, food processing, air conditioning, refrigeration, and medicine [7]. Cellular materials are receiving renewed attention as structural, functional materials. They have unique thermal, acoustic, and energy-absorbing properties that can be combined with their structural efficiency, and many kinds of cellular materials have been tested as damping and energy absorbing materials [31]. Therefore, cellular solids have numerous applications and new cellular structures are being developed continuously.

1.4 Statement of Purpose

To date, open cell corrugated cellular solid structures made from woven wires have not been widely studied or utilized. The objective for this work is to develop methods for fabricating open cell corrugated test samples from woven wire meshes, obtain mechanical properties including the compressive yield strength, and compare the tested mechanical properties to model predictions.

Several different samples will be fabricated over a range of relative density and pore size. The corrugated samples will differ based on different mesh size, wire diameter, opening width, and open area percentage. The compressive yield strength will be measured and compared to model predictions for open cell stochastic foams (Gibson-Ashby model, [2]). It is hypothesized that the Gibson-Ashby model can be used to predict the compressive yield strength of fabricated samples.

2. MECHANICAL BEHAVIOR PREDICTIONS

2.1 Architecture Types

Synthetic cellular solids generally fall into three categories: honeycombs, open celled stochastic foams and closed cell stochastic foams. Shapes of architectures commonly modeled are shown in Figs. 1-2, 1-3, and 1-4. Equations describing the relative density and plastic collapse for open cell structures using the Gibson-Ashby model are presented in the next section.

2.2 Methodology

The mechanical behavior of cellular solids can be modeled by idealizing the observed structures, characterizing the cell wall or strut properties, and analyzing the mechanisms by which the cell walls or struts deform [2, 10]. The properties of cellular solids are influenced by their relative density and morphology (open cell, closed cell), as well as the properties of the cell walls or struts [24].

Cellular solids have physical, mechanical, and thermal properties that are measured by similar methods as those used for fully dense solids. Four key properties are normally reported: density, thermal conductivity, Young's modulus, and compressive yield strength [2]. The useful properties of cellular solids depend on the material from which they are made, their relative densities, and their internal geometrical structure [32]. For metallic foams, low density, high strength and stiffness, good damping and energy absorbing capabilities, non-flammability, and the possibility for optimization are some of the positive attributes.

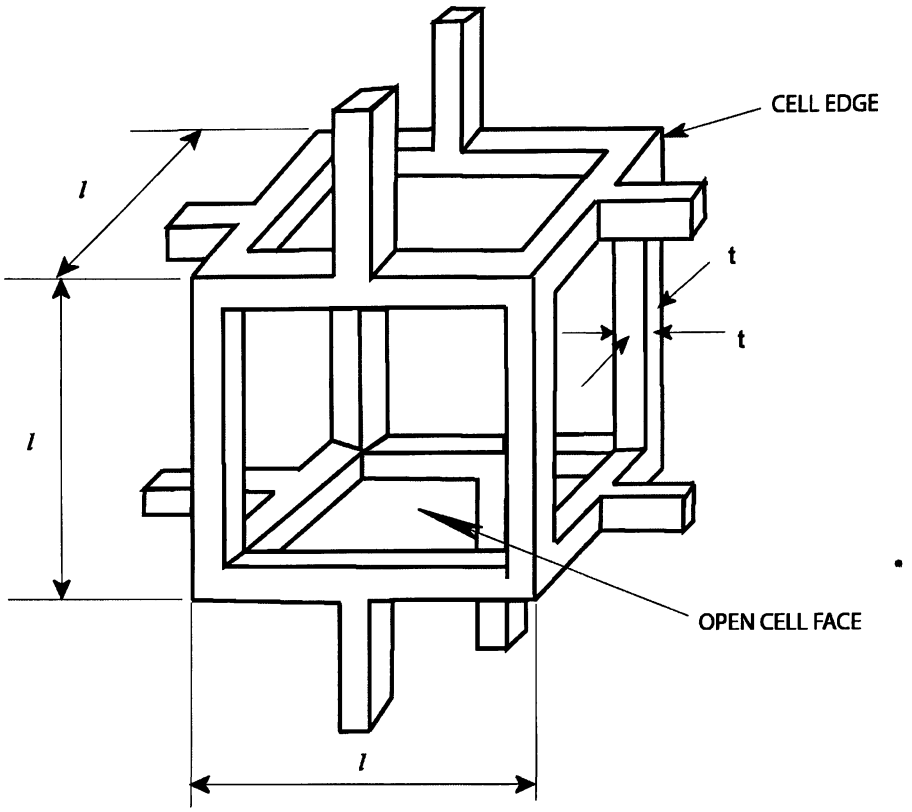

Figure 2-1. A cubic model for the open cell stochastic foam (edge length, *l*, edge thickness, *t*) [2].

2.3 Relative Density Predictions

Properties depend on the microscopic struts and plates that make up the cell edges and faces, and the way these respond to load, transmit heat, or dissipate energy. Because most engineers cannot expect to have reliable information regarding the exact cell wall thickness distribution for the foams they use, they usually make approximations and develop equations that relate average cell dimensions and shape to the density. The simplest approximations are reported herein.

For honeycombs [2];

$$\frac{\rho^*}{\rho_s} = C_1 \frac{t}{l} \tag{2-1}$$

where, ρ^* is the density of the cellular solid, ρ_s is the density of the wall or strut material, t is the thickness of the wall or strut material, l is the cell edge length, and C_1 is a numerical determined from experiment.

For open cell foams, if the strut thickness t is much less than the cell edge length l, ($t << l$), it implies that the relative density is low (See Fig. 2-1) [2]:

$$\frac{\rho^*}{\rho_s} = C_2 \left(\frac{t}{l}\right)^2 \tag{2-2}$$

Thus, the relative density for an open cell foam, Eqn. 2-2, is correlated with the edge thickness squared divided by the edge length squared.

For closed cell foams with faces of side l and uniform wall thickness t [2]:

$$\frac{\rho^*}{\rho_s} = C_3 \frac{t}{l} \tag{2-3}$$

where C_1, C_2, and C_3 are numerical constants, near unity, that depend on the details of the cell shape. These constants are normally determined from experimental measurements.

2.4 Mechanical Behavior Predictions

Based on concepts from Gibson-Ashby [2], the mechanical behavior for open cell foams previously shown in Fig. 2-1 will now be reviewed. Assumptions about the models will be described. Only plastic collapse will be discussed. Figure 2-2 shows a demarcation between open cell and closed cell foam models owing to differing physical mechanisms.

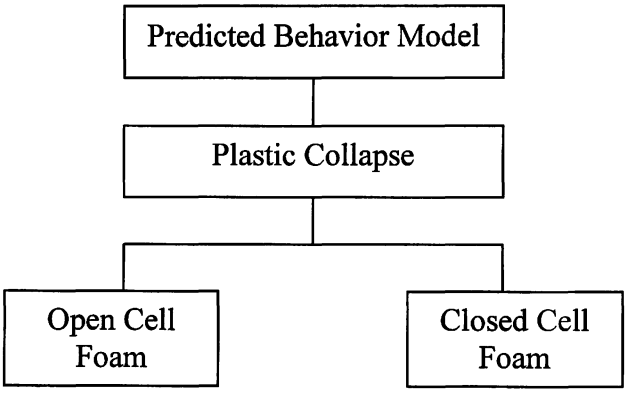

Figure 2-2. The predicted behavior model flow chart.

2.4.1 Plastic Collapse of Open Cell Stochastic Foams

Plastic collapse takes place when the moment due to a force F (See Fig. 2-3) exceeds the fully plastic moment of the cell edges [2].

$$M_p = \frac{1}{4}\sigma_{ys}t^3 \tag{2-4}$$

where M_p is the fully plastic moment of the cell edges, t is a thickness of beam with square cross section (See Fig. 2-1), and σ_{ys} is the yield strength of the cell wall material.

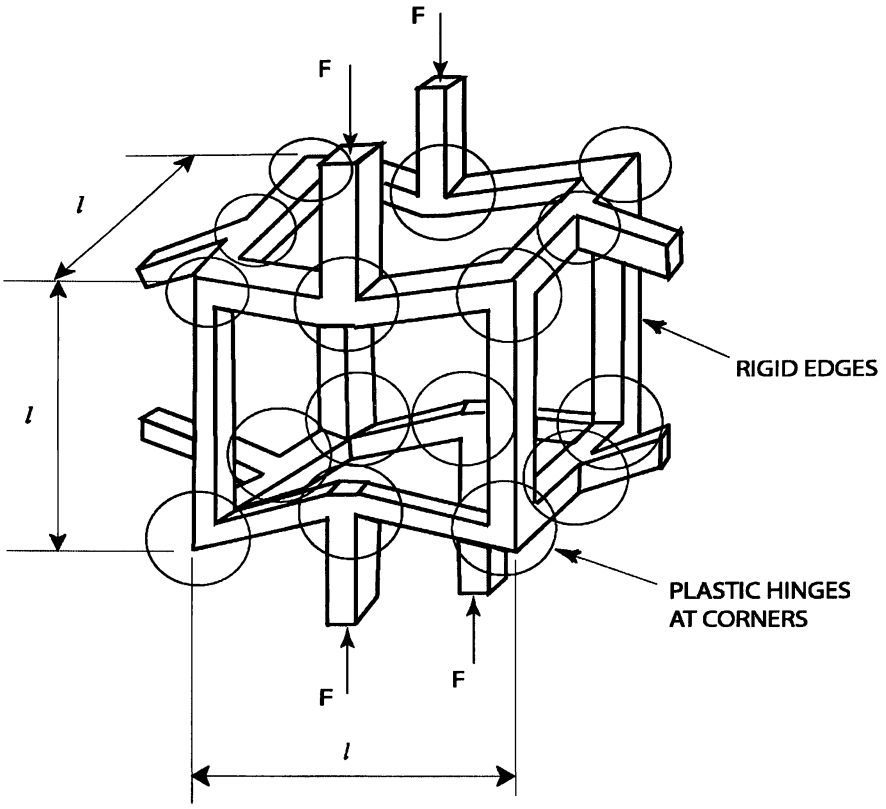

Figure 2-3. The formation of plastic hinges in an open cell foam.

If the force F has a component normal to the cell edge of length l, the maximum bending moment is proportional to Fl. The stress on the foam is proportional to F/l^2. Combining the results gives the plastic-collapse strength of the foam:

$$\sigma^*_{pl} = C\frac{M_p}{l^3} \tag{2-5}$$

where C is a constant based on the different sizes of cells in the foam.

Using $C_2 = 1$ in Eqn. 2-2 gives

$$\frac{t}{l} = \sqrt{\frac{\rho^*}{\rho_s}} \tag{2-6}$$

If Eqn. 2-4 is substituted into Eqn. 2-5, then [2]

$$\frac{\sigma_{pl}^{*}}{\sigma_{ys}} = \frac{C}{4}\left(\frac{t}{l}\right)^{3} \tag{2-7}$$

Substituting Eqn. 2-6 into Eqn. 2-7 [2]

$$\frac{\sigma_{pl}^{*}}{\sigma_{ys}} = \frac{C}{4}\left(\frac{\rho^{*}}{\rho_{s}}\right)^{\frac{3}{2}}$$

Then,

$$\frac{\sigma_{pl}^{*}}{\sigma_{ys}} = C_{4}\left(\frac{\rho^{*}}{\rho_{s}}\right)^{\frac{3}{2}} \qquad \text{(open cells)} \tag{2-8}$$

where $C_4 = C/4$.

2.5 Summary

In this work, the fabricated cellular structures will be assumed to have similar open cell architecture to those described above allowing comparison to open cell foam models. Open cell density and plastic collapse will be addressed. The equations to be used are summarized in Table 1. These equations are based on open cell stochastic foams only.

	Open cell stochastic foam	
Relative density	$\rho^*/\rho_s = (t/l)^2$	(Eqn. 2-2)
Plastic collapse	$\sigma^*_{pl}/\sigma_{ys} = C_4(\rho^*/\rho_s)^{3/2}$	(Eqn. 2-8)

Table 1. Equations for open cell relative density and plastic collapse.

3. EXPERIMENTAL

The objective of this chapter is to present a method for fabricating open cell corrugated test samples using woven wire meshes. The materials to be used are type 304 stainless steel woven wire cloth, a brazing alloy (Lithobraze 925), Argon gas (Ar, 99.995% purity), Grade 1 titanium powder, ceramic paper (Al_2O_3 fiber), stop-off material (Nicrobraze green), and methanol. The major experimental equipment is a furnace operating at a brazing temperature of 971°C (1780°F). Each of these will now be further explained.

3.1 Metal Textiles

Wire mesh has found numerous applications over a wide variety of industries. These are economical, can have a large open area (high porosity), are lightweight, attractive in appearance, versatile, handle easily, cut and shear easily, and are available in a wide variety of styles and materials. Wire mesh are used for grills, machine guards, lockers, security fences, pallets, bins, infill panels, baskets, dryer trays, strainers, filters, fan guards, speaker covers, fencing, window guards, gates, etc. [35].

The basic equations for describing the density and porosity within a wire mesh can be essential when helping to select the right product. Wire spacing, opening size, and wire diameter are often important considerations for a design decision. Figure 3-1 shows a typical plain square woven wire cloth where d is wire diameter and w is opening width.

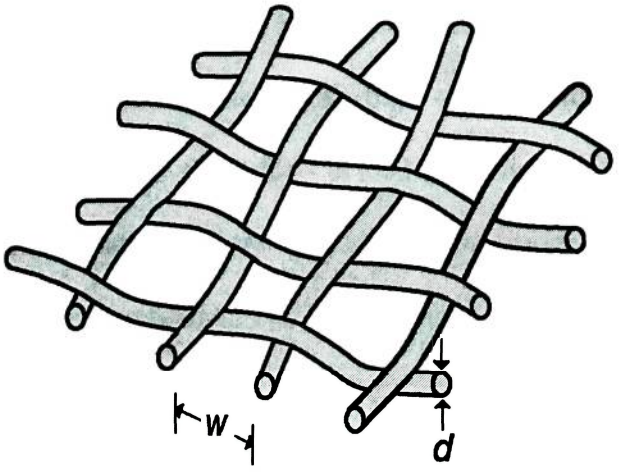

Figure 3-1. Wire diameter and opening width for woven wire cloth.

For computing and selecting a certain percent open area for a wire mesh product, the following equation can be used [40].

$$\% \text{ Open Area} = \frac{w^2}{(w+d)^2} \times 100 \tag{3-1}$$

The relative density of the mesh is given by [36, 37]

$$\frac{\rho^*}{\rho_s} = \frac{\pi d}{4(w+d)} \tag{3-2}$$

Most companies list wire mesh products based on the parameters shown in Fig. 3-1 along with the open area percentage (%).

Wire mesh products are made from many types of materials and in many different forms; plain square woven wire cloth, welded wire cloth, crimped metal wire cloth, etc. Perforated products, such as perforated metal and plastic sheets, woven and molded thermoplastic mesh, are similarly categorized. Other forms of wire mesh products include square hole, mesh fence, barbed wire, welded wire mesh, and so on [38]. Woven wire mesh and wire cloth can be woven in different ways - Dutch twill weave, heddle

weave, plain weave, plain Dutch weave, reverse Dutch weave, and twill weave. Common base materials include cold-rolled steel, high carbon alloy steel, galvanized steel, stainless steel, PVC (polyvinyl chloride) - coated galvanized steel, vinyl - coated galvanized steel, plain steel, aluminum, brass, bronze, copper, monel, nickel chromium, nichrome, nylon, polyester, polypropylene, etc. Less commonly woven are more exotic materials like titanium alloys.

The cost for wire mesh varies depending on the base material type, size of mesh, wire diameter, opening width, and the size of the sheets. For example, the current cost for type 304 stainless steel, with size ranging from 0.03937 mesh/mm (1 mesh per inch) to 25 mesh/mm (635 mesh/inch), is from $17 to $653 per square foot [38]. A piece of plain square woven Grade 5 titanium (Ti-6Al-4V) 609.6 mm (24 in) wide by 254 mm (10 in) long (in stock), with 1.9685 mesh/mm (50 mesh/inch), 0.1016 mm (0.004 in) wire diameter, 0.4064 mm (0.016 in) opening width and 64 % opening area, is about $600 [39]. The cost of a similar Grade 1 titanium alloy is about $90 per square foot [40]. Note that the cost for more common alloys are significantly less than for rare or exotic alloys.

3.2 Base Materials

Owing to the availability, corrosion resistance, low cost, high temperature capability (rated from 1010°C to 1211°C), high yield strength, high stiffness, and ability to be bonded, type 304 stainless steel was selected as the base material for this investigation. Table 2 lists several key properties for this alloy. A typical type 304 stainless steel mesh is shown in Fig. 3-2. Details of the wire mesh that were used for making test samples are listed in Table 3 where as-received relative density has been calculated using Eqn. 3-2. The mesh was plain square woven and made from type 304

stainless steel. These were purchased from McMaster-Carr Supply Company (Atlanta, GA) [41].

Wrought alloy	Density (g/cm^3)	Young's modulus [GPa]	Yield strength [MPa]	Yield strain
Type 304 stainless steel (annealed)	8.0	193	205	0.0011

Table 2. Properties for type 304 stainless steel [38].

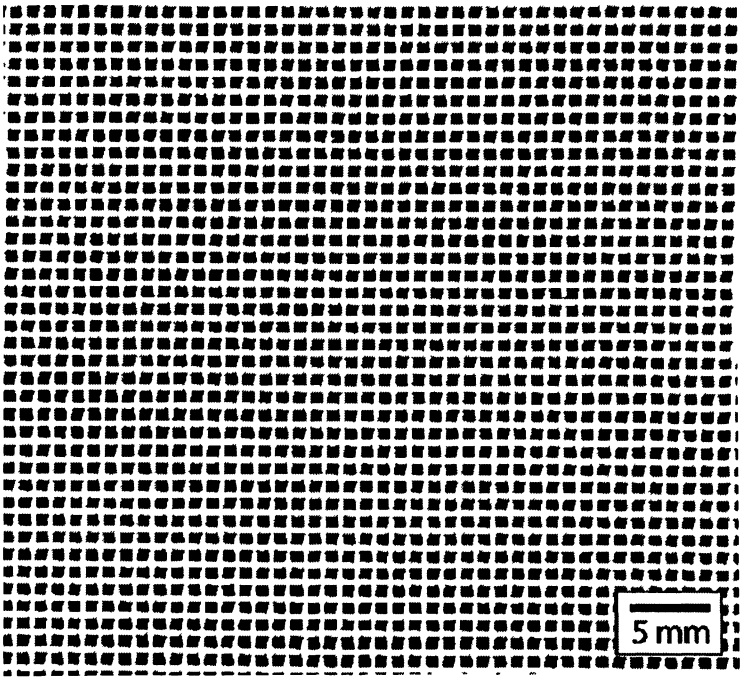

Figure 3-2. Type 304 stainless steel woven wire cloth.

Sample Name	Mesh per		Wire dia.		Opening width		Density of mesh
	(in)	(mm)	(in)	(mm)	(in)	(mm)	ρ^*/ρ_s
A	24	0.945	0.0140	0.356	0.0280	0.7112	0.262
B	26	1.024	0.0075	0.191	0.0318	0.8084	0.150
C	26	1.024	0.0075	0.191	0.0310	0.7874	0.153
D	28	1.102	0.0100	0.254	0.0260	0.6604	0.218
E	32	1.260	0.0065	0.165	0.0250	0.6350	0.162
F	40	1.575	0.0095	0.241	0.0160	0.4064	0.293
G	50	1.969	0.0090	0.229	0.0110	0.2794	0.353
H	80	3.150	0.0070	0.178	0.0060	0.1524	0.423

Table 3. Details for test samples.

3.3 Crimping

Figure 3-3 shows the idea of how to make inexpensive, corrugated porous shapes using woven wire meshes. Crimping implies to press or pinch into small regular folds or ridges (e.g., *crimp a pie crust)*, to bend or mold (leather) into shape, or to cause (hair) to form tight curls or waves [1]. It is postulated that by corrugating wire mesh and bonding, that relative density of the resulting 3-D structures will substantially reduced while maintaining good strength. More so, than normal woven shapes that are not bonded. This method and thought will be used to create new cellular structures.

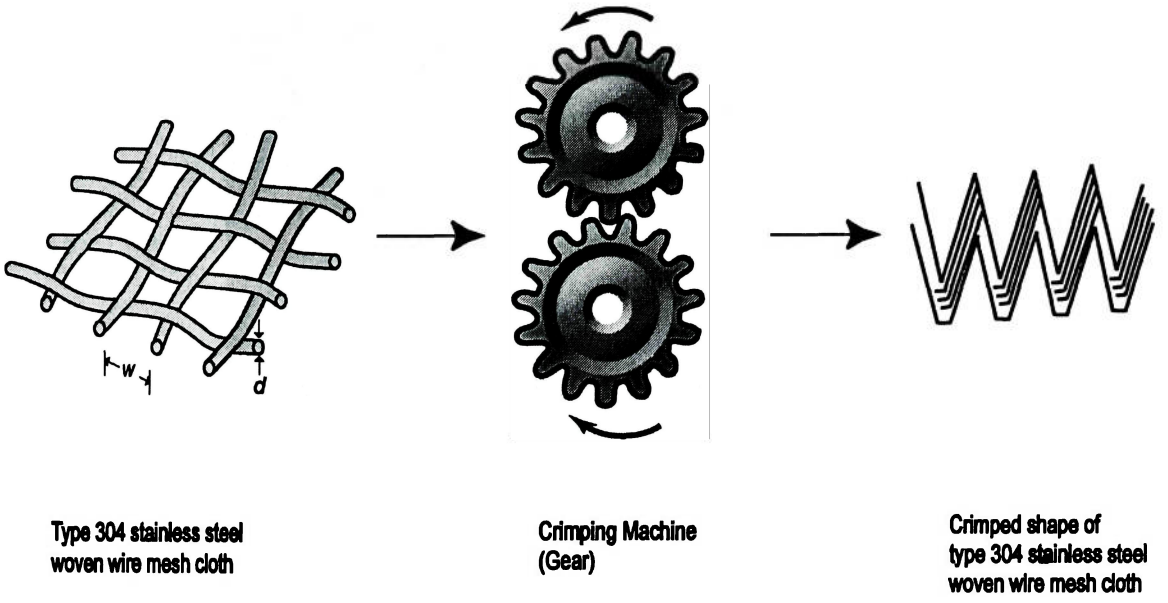

Figure 3-3. A diagram for making a corrugated shape.

Figure 3-4 shows the crimping machine used to make the corrugated shapes. The left side of the picture shows the intersecting spur gears. When the handle on the right side is turned, the gear moves, grabbing the mesh between and drawing it in to crimp it.

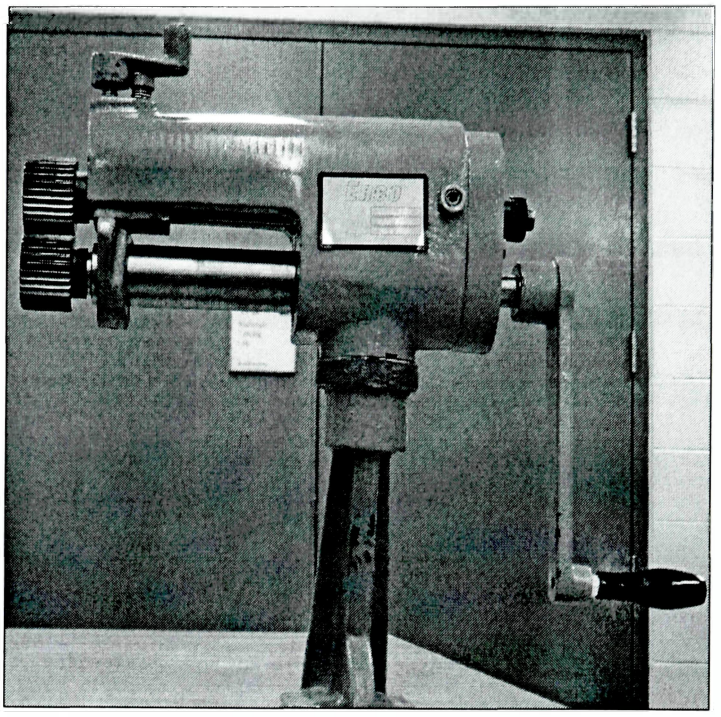

Figure 3-4. Crimping machine used for corrugating.

To make the individual corrugated ply, 30 mm x 61 mm (12 in x 24 in) woven wire mesh sheets made from type 304 stainless steel were used. Before sample fabrication, each woven wire sheet and gear part in contact with the mesh were cleaned to remove dirt, dust, fingerprints, etc., on the surface of the material. Rubber gloves were used when handling to protect against fingerprints. The initial cleaning procedure is outlined below:

1. Cut the stainless steel mesh into 20 sheets, each 50.8 mm (2 in) by 50.8 mm (2 in).
2. Remove oil from the surface of the mesh with a degreasing agent.
3. Remove oil from the crimping machine spear gears.
4. Cleanse the gears using methanol (CH_3OH).
5. Wait five to ten minutes for the methanol to evaporate.

Figure 3-5 shows the wavy shape of wire mesh after cleaning and crimping. It is considered to be corrugated shape owing to its geometry. With this method, an essentially 2-D shape (wire mesh) has taken on 3-D dimensions. Each sheet of mesh listed in Table 3 was subjected to this procedure prior to laminating and bonding. Sample A and B have 10 ply thickness. Sample C, D, E, F, G, and H have 20 ply thickness.

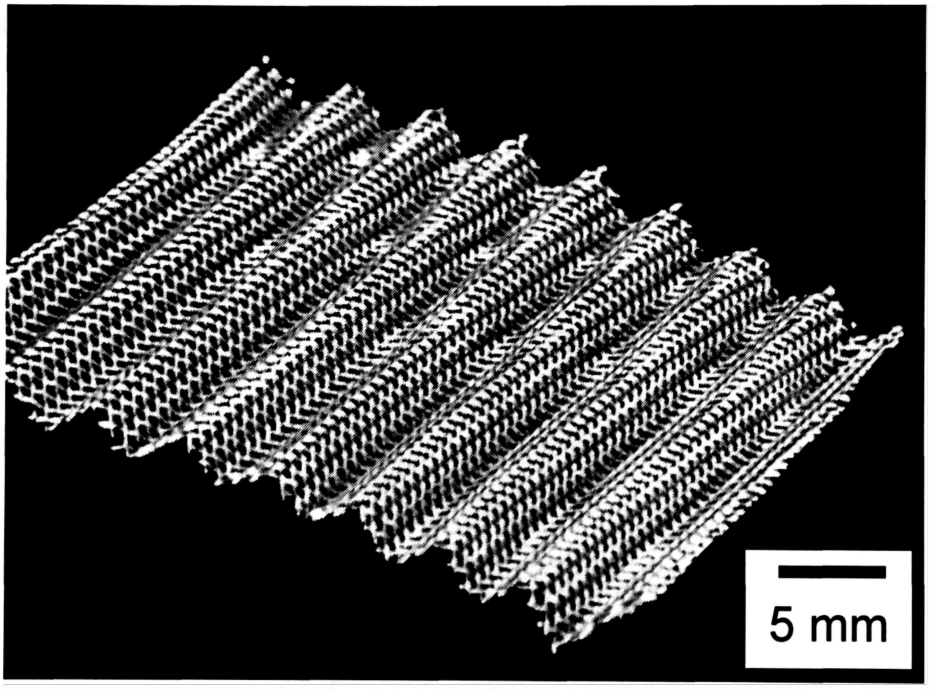

Figure 3-5. Corrugated shape of woven mesh.

3.4 Lamination Methodology

To fabricate thick porous samples from relatively thin corrugated meshes, an inert gas brazing approach was used to bond the crimped mesh to one another. To apply the brazing alloy, rods of brazing alloy (lithobraze 925) were cut to 50.8 mm (2 in) lengths per rod. About 7-8 lithobraze rods were needed for each corrugated woven mesh ply. 70-80 lithobraze rods were needed for samples A and B. 140-160 lithobraze rods were needed for samples C, D, E, F, G, and H. Figure 3-6 shows the assembly.

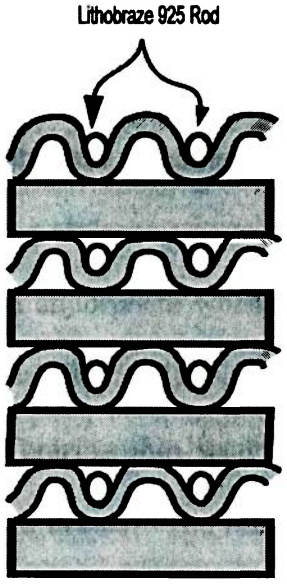

Figure 3-6. Lamination assembly.

3.5 Lithobraze 925

Lithobraze 925 consists of 92.5Ag-7.3Cu-0.2 Li by wt.%. Because of the 0.2% lithium, lithobraze 925 has desirable melting, liquidus, and brazing properties. Physical properties for this alloy are indicated in Table 4. These include a silver-white color, a

melting point of 760°C (1400°F), a liquidus of 890°C (1635°F) and a density of 10.12 g/cm^3 (5.33 Troy oz./in^3).

Composition	Ag-7.3Cu-0.2Li
Color	Silver-white
Melting point	760°C (1400°F)
Liquidus	890°C (1635°F)
Density	10.12 g/cm^3 (5.33 Troy oz./cu.in.)
Min. brazing temp.	900°C (1652°F)
Max. operating temp.	260°C (500°F)

Table 4. Lithobraze 925 composition and physical properties [42]

Lithobraze 925 is commonly used for brazing honeycomb panel sections and general-purpose furnace brazing of stainless steels where flux must be avoided. This alloy has been widely used for brazing airframe structures made of stainless steel [42]. Argon (Ar) gas is the most common atmosphere when bonding with this alloy. The minimum rated brazing temperature is 10°C (50°F) above the flow point. These types of alloys are particularly adaptable to brazing thin sections of stainless steels because negligible interaction between the two occurs. The lithobraze 925 was obtained from Lucas-Milhaupt, Inc., Cudahy, WI.

3.6 Sample Fabrication

All materials used during the fabrication process were first cleaned following the steps outlined earlier. Figure 3-7 shows the method used for obtaining a high temperature Ar brazing atmosphere. The Ar gas pressure was kept at 34.5-70 kPa (5-10 psi) with most samples at 40 kPa (5.8 psi). Both top and bottom plate sizes are 12.7 mm (0.5 in) thick and 101.6 mm x 101.6 mm (4 in x 4 in). The hollow body is 101.6 mm x

101.6 mm x 203.2 mm (4 in x 4 in x 8 in) with thickness of 6.35 mm (0.25 in). Ceramic paper was used to preventing sticking. Pure titanium (Ti) powder (Crucible Research, Pittsburgh, PA) was used for protecting the sample from oxygen. A powder support was used for preventing Ti powder from dropping onto the laminated sample. A weight plate was used to compress the ply together for brazing. A support was used for holding the crimped mesh ply to ensure a good sandwich shape. Nicrobraze green stop-off (Wall Colmonoy Corp., Madison Heights, MI) was used to prevent sample sticking at the bottom of the cup. These will be described in more detail in the following section.

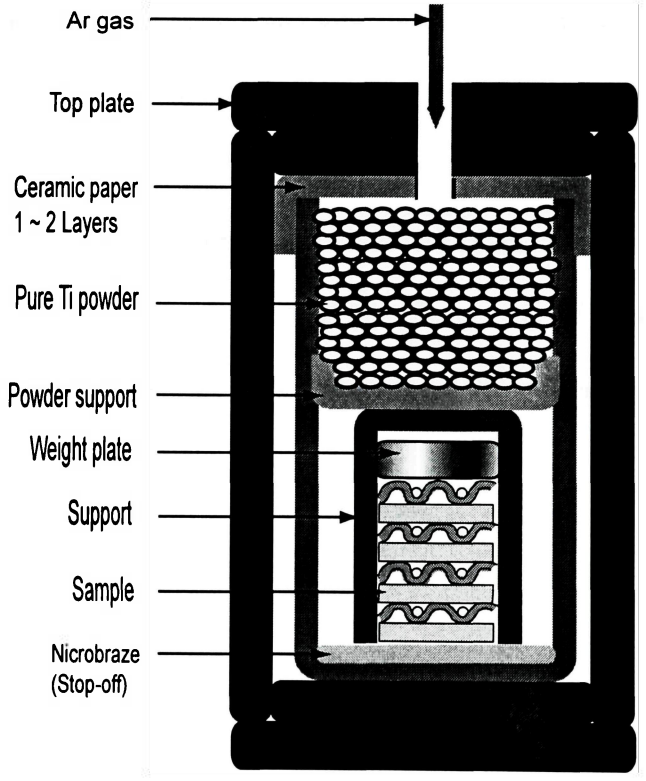

Figure 3-7. Method for obtaining a high temperature Ar brazing atmosphere.

A type 304 stainless steel cup was used as the brazing container. It had a diameter of 64.7 mm (2.5 in) and a height is 87.2 mm (3.4 in). Additional details are given in Table

5. Table 5 shows cup, support, and powder support. 304 SS implies type 304 stainless steel

	Mesh per (mm)	Material used	Wire dia. (mm)	Opening width (mm)	Open area (%)	Outer dia. (mm)	Outer height (mm)	Inner dia. (mm)	Inner height (mm)
Cup		304 SS				64.7	87.2	62.9	85.4
Support	0.79	304 SS	0.46	0.81	41.0				
Powder support	3.94	304 SS	0.11	0.15	30.3				

Table 5. Data for brazing process equipment.

The next step was furnace preparation, Figs. 3-8 through 3-13. For making large samples, this cup needed to be a large size and also fit on the inside of the stainless steel protective box shown in Fig. 3-7. First, the bottom of this cup had Nicrobraze green stop-off applied to it, as shown in Fig. 3-8. This ceramic based material is designed to endure high temperatures due to special physical/chemical characteristics. Its low boiling temperature of 56°C to 176°C (132~349°F) and specific gravity of 1.16 give it a slow evaporation rate. It prevents the sample from sticking to the bottom of the cup during brazing at 925°C (1700°F).

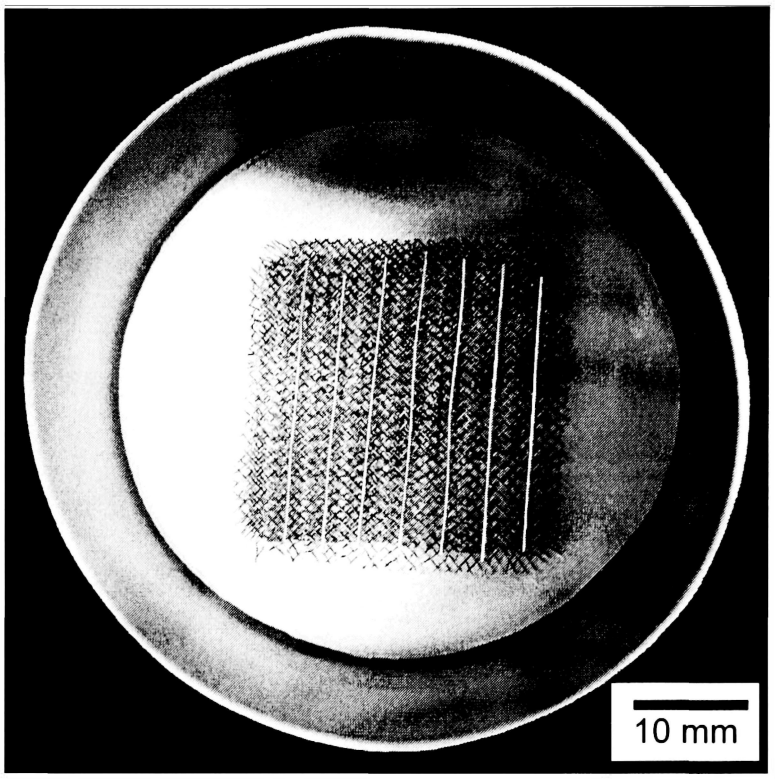

Figure 3-8. Lamination. Nicrobraze was applied to the bottom and then crimped mesh layers were added. Lithobraze 925 wires are seen within each valley.

Each crimped sheet with lithobraze wires in the valleys was added to this cup at ±90 degree orientations. A stainless steel (type 304) circular plate was used as a top weight to push the sandwich layers into contact with one another. This circular plate, shown in Fig. 3-9, had a mass of 307 grams.

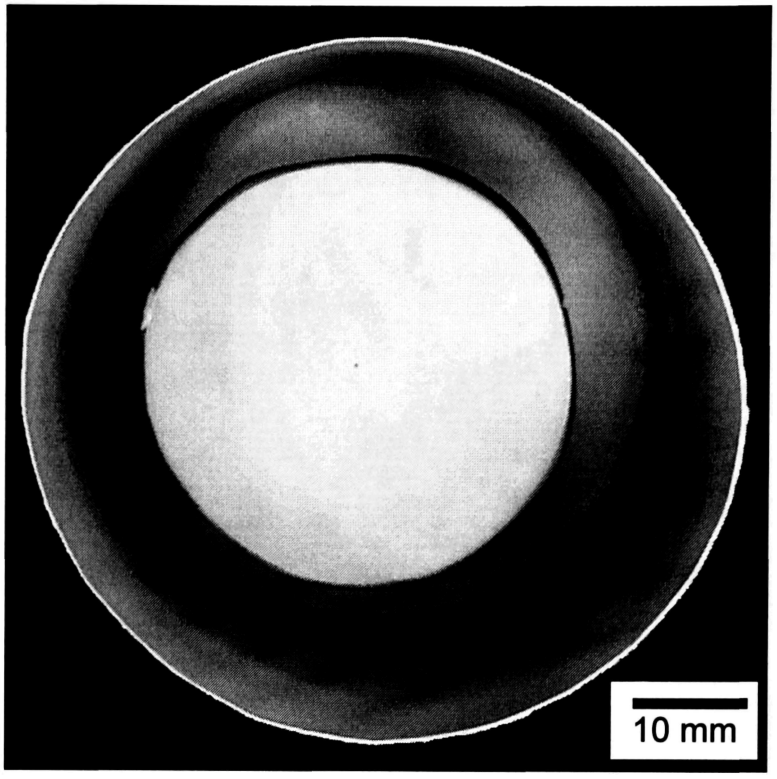

Figure 3-9. Circular type 304 stainless steel plate added to press sample layers together.

Next, a wire mesh stand was placed around the stack to support the weight of the Ti getter powder. Fig. 3-10 shows the mesh stand and data for it is listed in Table 6 in the support row.

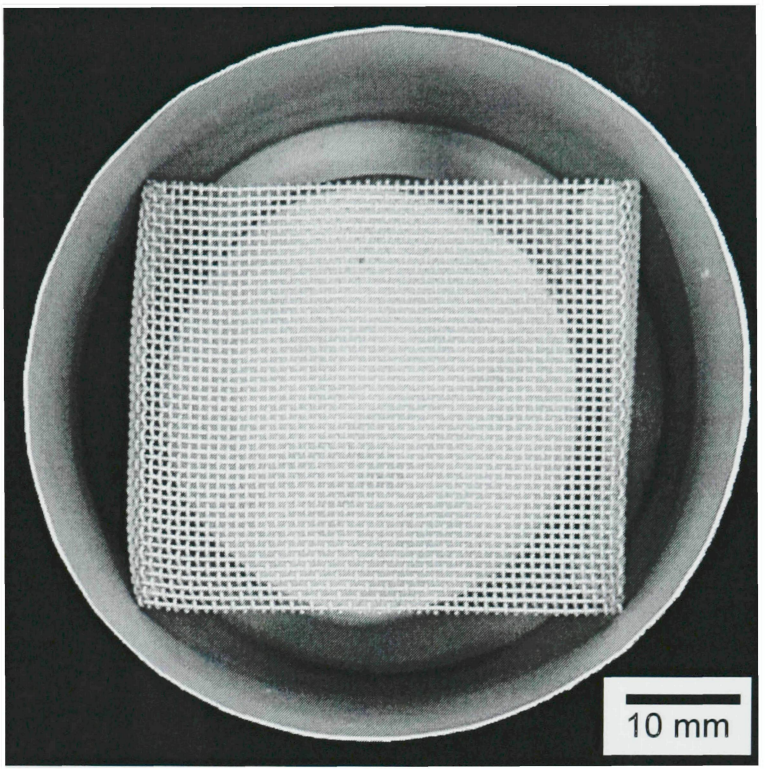

Figure 3-10. Mesh stand used to support the weight of getter powder.

Grade 1 Ti powder was used as the getter material. The powder size was –20/+35 and was obtained from Crucible Research, Pittsburgh, PA. The Ti powder size ranged from greater than 1.378 mesh/mm (35 mesh/inch) to less than 0.787 mesh/mm (20 mesh/inch). To support the powder, type 304 stainless steel mesh of size 3.94 mesh/mm (100 mesh/inch) was placed on top of the mesh stand. The fine mesh size prevents most of the Ti powder from entering the brazing area. The mesh sheet is shown in Fig. 3-11 and its data is in Table 6.

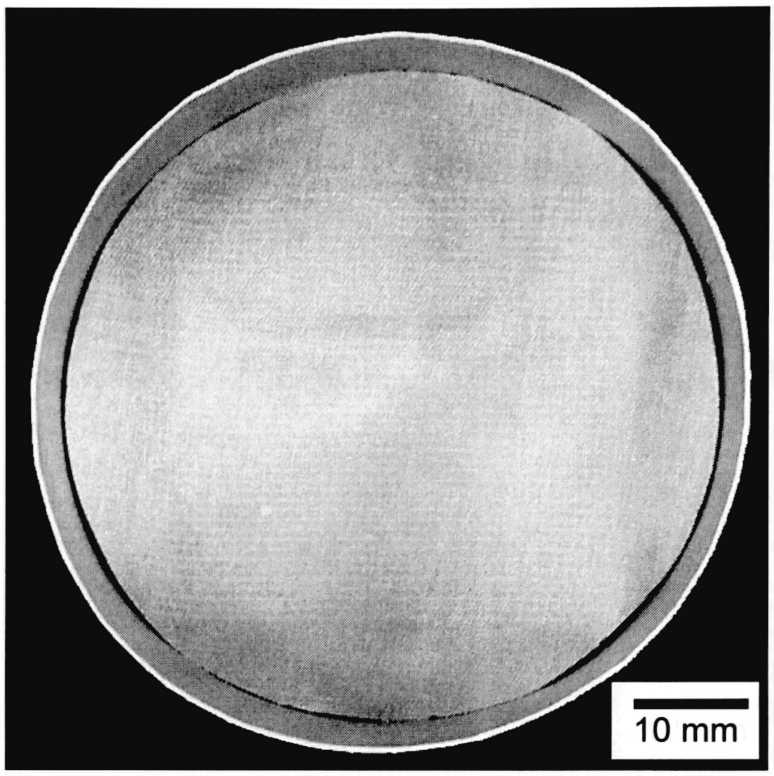

Figure 3-11. Circular mesh sheet used for supporting the Ti powder.

Grade 1 Ti powder has low strength and low oxygen content. Owing to its high reactivity with oxygen at elevated temperatures, it is often used for protective environments. Without protection from oxygen, the test samples and brazing alloy would easily oxidize at the brazing temperature rendering them useless. Even a little oxygen inside the brazing area can lead to problems. Therefore, protecting from oxygen is a very important step during fabrication. A picture of the brazing cup with protective Ti powder is shown in Fig. 3-12.

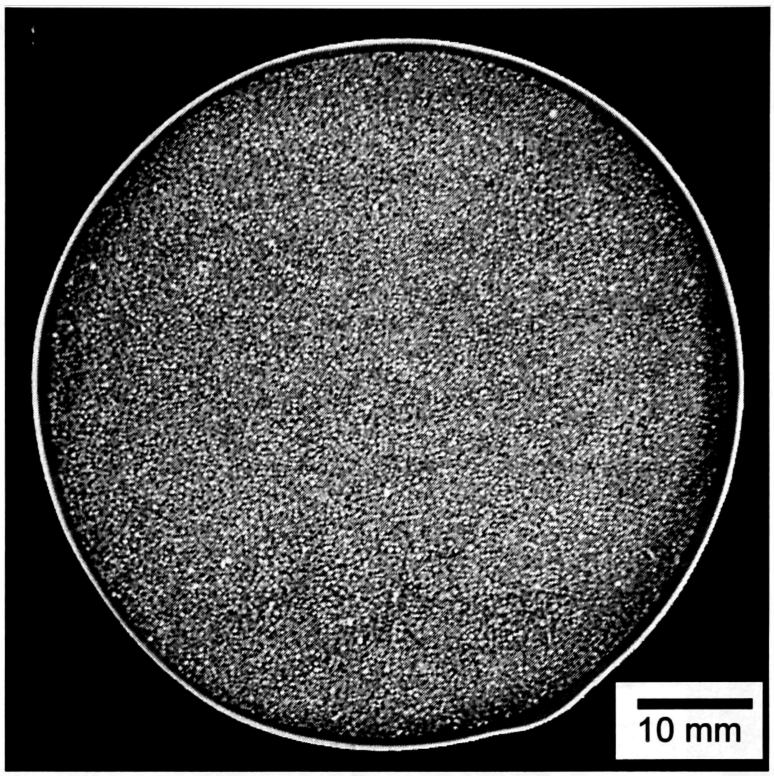

Figure 3-12. Grade 1 Ti powder used to protect from oxygen.

After completing these steps, the cup was placed into the Ar atmosphere protective box also made from type 304 stainless steel. The box is constructed using a machined top, bottom, and hollow rectangular body part. Ceramic paper was used as a gasket for gaps where parts of the protective box were joined. It helped prevent oxygen from entering into the box and allowed a positive Ar pressure to be maintained within. This binderless ceramic fiber paper is made from Al_2O_3 fibers, can endure a very high temperature, and is white in color. The paper is highly flexible so it is easy to cut, wrap, and form. It also has an excellent resistance to most chemicals. It is used for combustion chamber liners, basket and tray linings, thermal and electrical insulation, separators to prevent sticking, and as a parting agent in brazing and heat-treating operations [38].

This assembly was then placed into a furnace for brazing as shown in Fig. 3-13. Heating under flowing Ar occurred at ~925°C (1700°F) for a hold time of approximately 30 minutes. The Ar gas pressure was kept in the range of 34.5 kPa to 70 kPa (5-10 psi). Once 30 minutes had elapsed, heating was ceased and the furnace door was opened for cooling. The sample was allowed to cool to ~204°C (400°F) or less under the protective Ar atmosphere. If the Ar gas is turned off while the sample is still hot, oxygen can enter into the protective box and cup, and readily contaminate the sample.

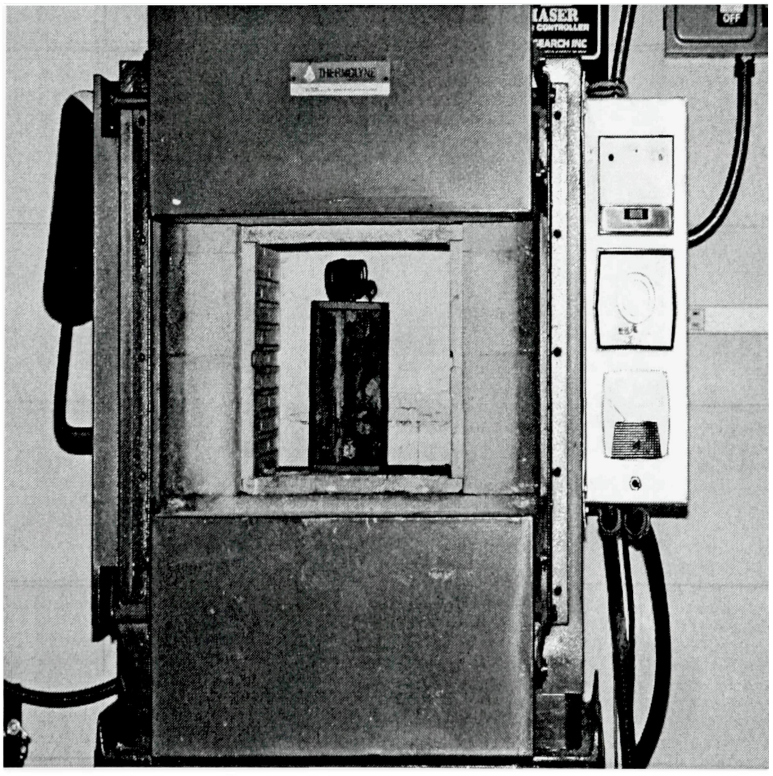

Figure 3-13. Furnace used for brazing and the protective box inside it.

After cooling below ~204°C (400°F), the protective steel box was removed from the oven. The assembly was disassembled, the cellular test sample was removed and then placed under flowing tap water for final cooling. A picture of a typical test sample (after

water lubricated cutting and sanding) is shown below in Fig. 3-14. Fig. 3-15 is a close up view showing the bottom of the sample. In Fig. 3-15, the silver color dots are melted portions of the brazing alloy, lithobraze 925. This picture shows that the sample bonding procedure has worked.

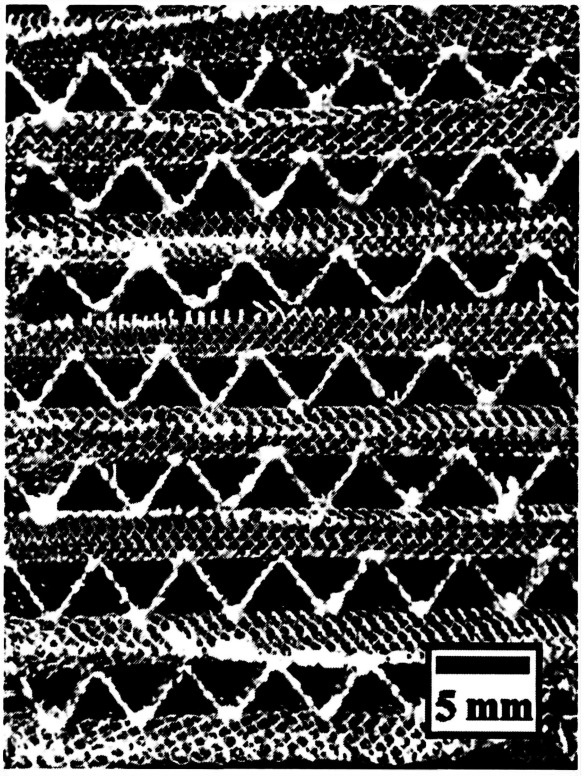

Figure 3-14. Fabricated sample.

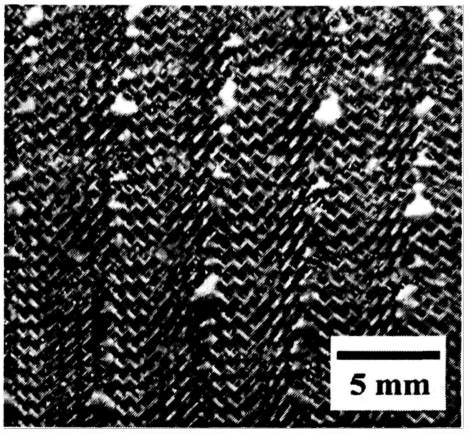

Figure 3-15. Bottom view of sample after cooling.

Table 6 shows data for completed samples after fabrication. Sample dimensions were measured using a digital caliper and mass was measured using a digital mass scale. Sample mesh per mm ranged from 0.945 to 3.150. The laminated samples had volumes ranging from 22.29 cm^3 to 97.58 cm^3 and weights ranging from 9.0 g to 61.2 g. The densities ranged from 0.307 g/cm^3 to 0.726 g/cm^3. Thus, based on volume, weight, and type 304 stainless steel density, laminated samples had relative densities ranging from 0.038 to 0.091.

Sample	Mesh per		Laminated sample data							
	(in)	(mm)	Width (mm)	Length (mm)	Height (mm)	Area (mm^2)	Volume (mm^3)	Weight (g)	ρ (g/cm^3)	ρ/ρ_s
A	24	0.945	30.5	29.6	24.7	904.0	22292.5	9.0	0.404	0.050
B	26	1.024	35.5	31.9	25.2	1131.0	28468.0	10.2	0.358	0.045
C	26	1.024	37.8	46.5	25.1	951.0	44261.7	16.6	0.375	0.047
D	28	1.102	45.8	40.6	50.1	1859.3	93149.5	51.0	0.548	0.068
E	32	1.260	42.0	42.4	54.8	1782.1	97585.6	30.0	0.307	0.038
F	40	1.575	39.8	39.5	49.6	1573.3	73331.4	49.5	0.675	0.084
G	50	1.969	41.6	42.1	49.0	1751.4	85834.6	61.2	0.713	0.089
H	80	3.150	38.9	41.7	48.9	1623.4	79446.9	57.7	0.726	0.091

Table 6. Laminated sample data.

3.7 Relative Density Discussion

Figures 3-16 and 3-17 show the variation of wire mesh density before crimping. Figure 3-16 shows relative density of mesh as a function of wire diameter. Figure 3-17 shows relative density of mesh as a function of opening width. Relative densities range from 0.0382 to 0.0920, wire diameters range from 0.178 mm to 0.3556 mm while wire mesh sizes range from 9.5 pore/cm to 31.5 pore/cm. Figure 3-16 shows that relative density increases when wire diameter is increased for a given opening width. Figure 3-17 shows that relative density decreases when opening width is increased for a given wire diameter.

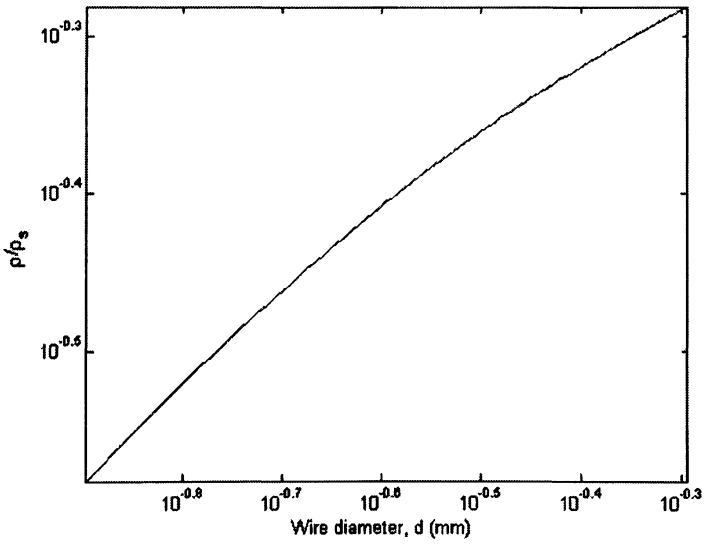

Figure 3-16. Relative density of mesh as a function of wire diameter for an opening width fixed at 0.254 mm.

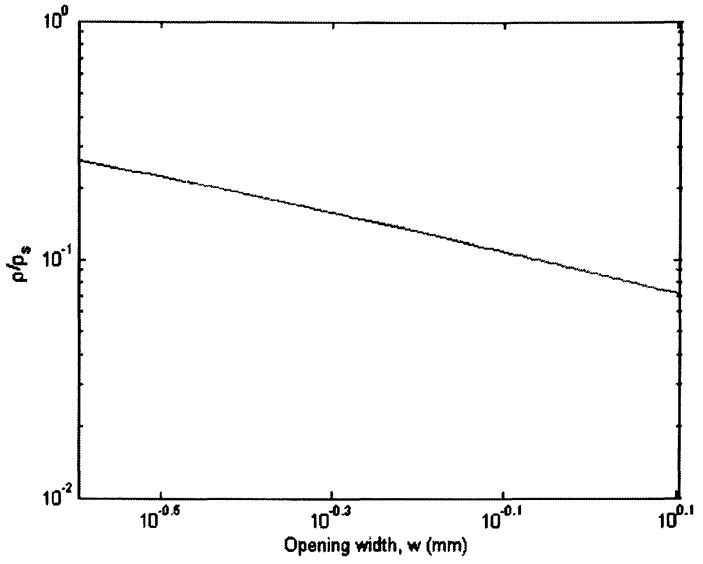

Figure 3-17. Relative density as a function of opening width for a wire diameter fixed at 0.127 mm.

Figure 3-18 demonstrates the relation between the mass of sample and the relative density. It shows that the relative density increases as the sample mass increases for a fixed sample volume. Figure 3-19 shows that relative density decreases with increasing volume for a fixed sample mass.

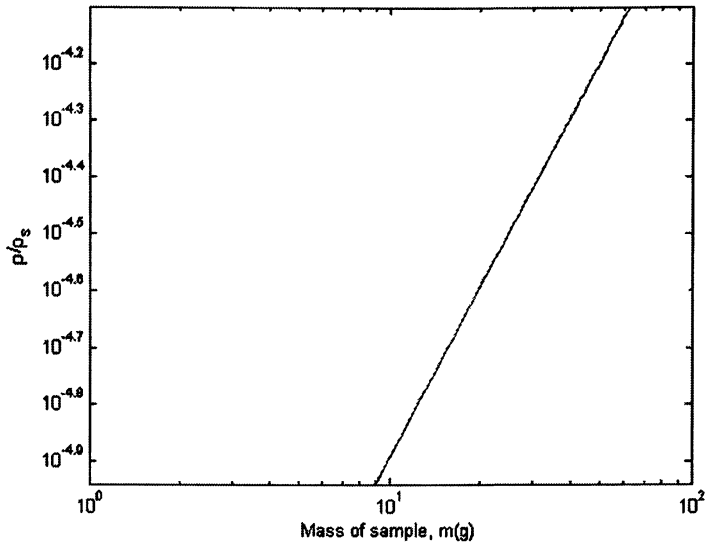

Figure 3-18. Relative density and mass of fabricated samples when volume is fixed at 22300 mm^3.

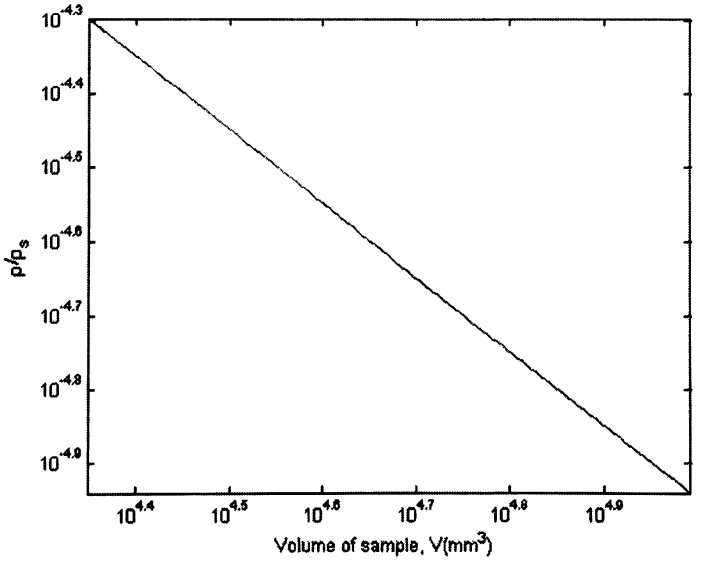

Figure 3-19. Relative density and volume of fabricated samples when mass is fixed at 9.0 g.

The relative density of woven wire cloth for the experiments ranged from 15% to 42.3% before crimping. After crimping, the relative densities for fabricated samples ranged from 3.8% to 9.1%. Therefore, the relative density of corrugated samples as compared to flat woven meshes has been reduced by 70% to 80%. Table 7 shows the relative density reduction. Wire mesh density has been significantly decreased by deformation in the out-of-plane-direction.

Sample	Relative density			
	Crimping		Reduction	
	Before	After	Δ	(%)
A	0.262	0.051	-0.807	-80.7
B	0.150	0.045	-0.701	-70.1
C	0.153	0.047	-0.693	-69.3
D	0.218	0.069	-0.685	-68.5
E	0.162	0.038	-0.763	-76.3
F	0.293	0.084	-0.712	-71.2
G	0.353	0.089	-0.748	-74.8
H	0.423	0.091	-0.785	-78.5

Table 7. Comparison of relative density.

4. MECHANICAL BEHAVIOR

4.1 Compressive Testing

This chapter describes mechanical behavior of compressive testing. After fabricating samples, mechanical tests were conducted using a Tinius-Olsen (Tinius-Olsen Corp, Horsham, PA) screw driven electromechanical testing machine, Fig. 4-1. This machine can be used for tension or compression testing. The applied forces were 3000 N, 15000 N, 60000 N, or 150000 N. The applied length changes were 12.5 mm, 50 mm, 250 mm, 500 mm, or 1250 mm.

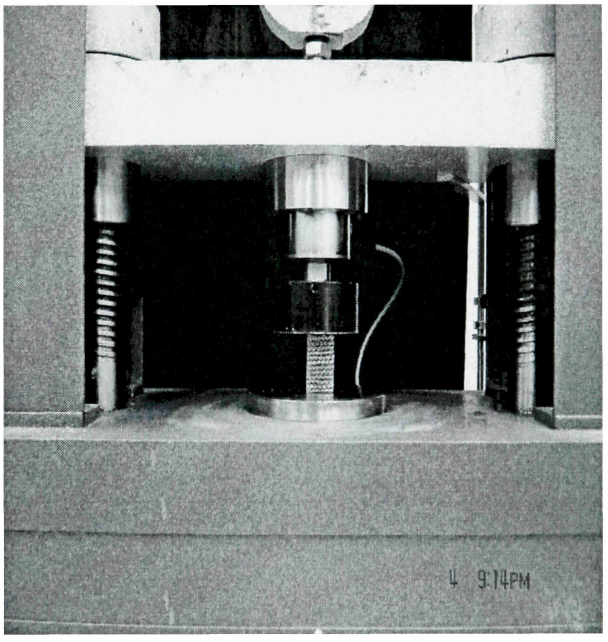

Figure 4-1. Compressive testing machine (settings: 3000 N, 50 mm).

This machine was set up such that the maximum applied force was 3000 N (y-axis on the graph), while the maximum change of length was 50 mm (x-axis on the graph) to accommodate anticipated values for the size and type of samples tested. When

performing quasistatic crushing tests, force vs. length was recorded. Before testing the fabricated cellular samples, blue styrofoam was used for practicing preparation runs. The blue foam samples had the same length, height, and area as test samples made from corrugated type 304 stainless steel. The machine was set up in the same fashion as expected for the final sample testing and runs were conducted to verify the functionality of the testing machine and method. To change from a force-length curve to a stress-strain curve, force was divided by sample area while strain was computed simply as the change in sample height divided by the original height.

4.2 Test Results

Figure 4-2 shows the compressive behavior for a corrugated cellular solid made from type 304 stainless steel. Strains ranging from 10% to 90% are shown at 10% increments.

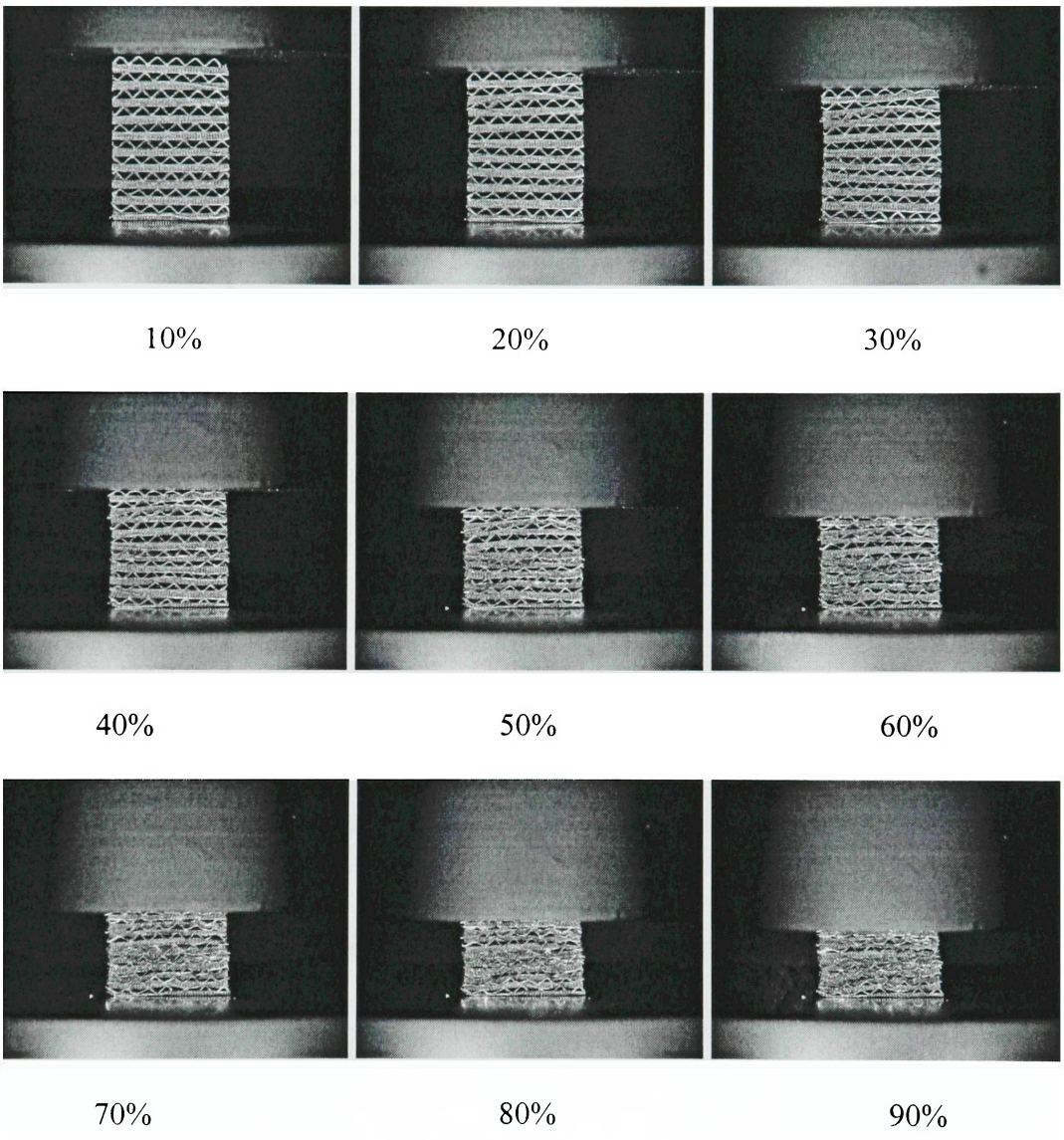

Figure 4-2. Compressive test results for sample G.

Figures 4-3 to 4-10, show the stress-strain curves for all test samples in order of increasing relative density. The relative density for each sample is shown in the left upper corner of each graph along with other important information.

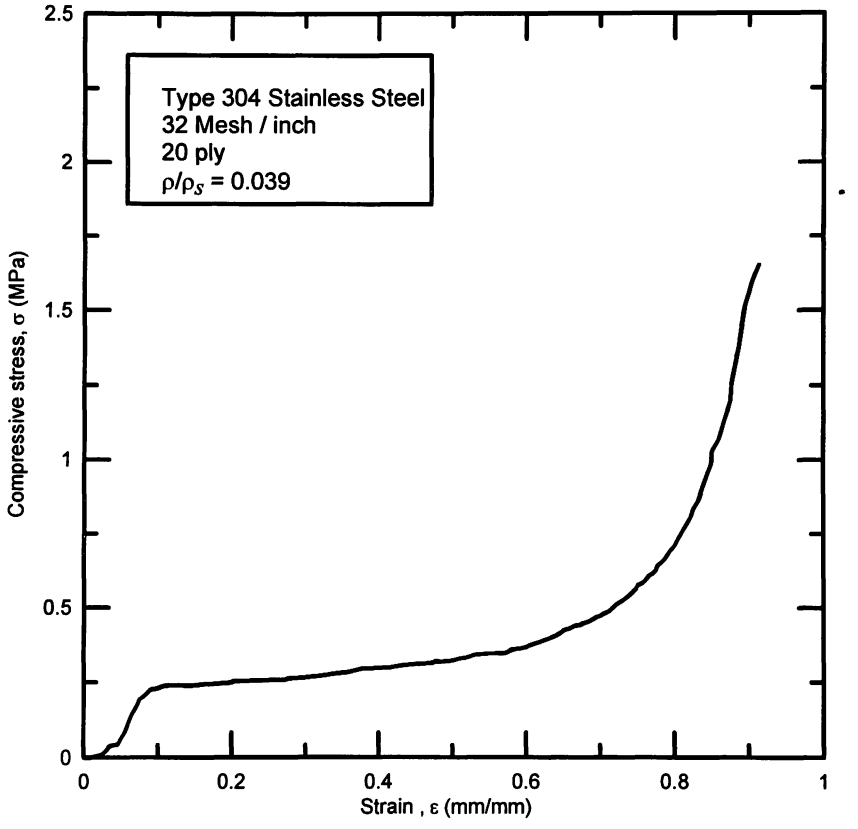

Figure 4-3. Stress-strain curve (sample E).

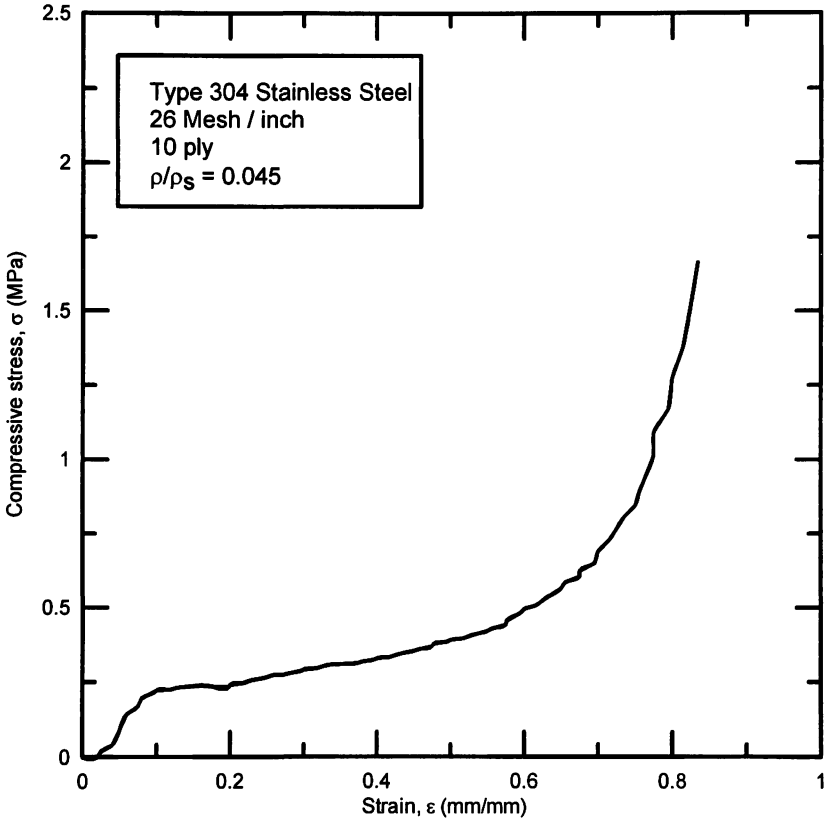

Figure 4-4. Stress-strain curve (sample B).

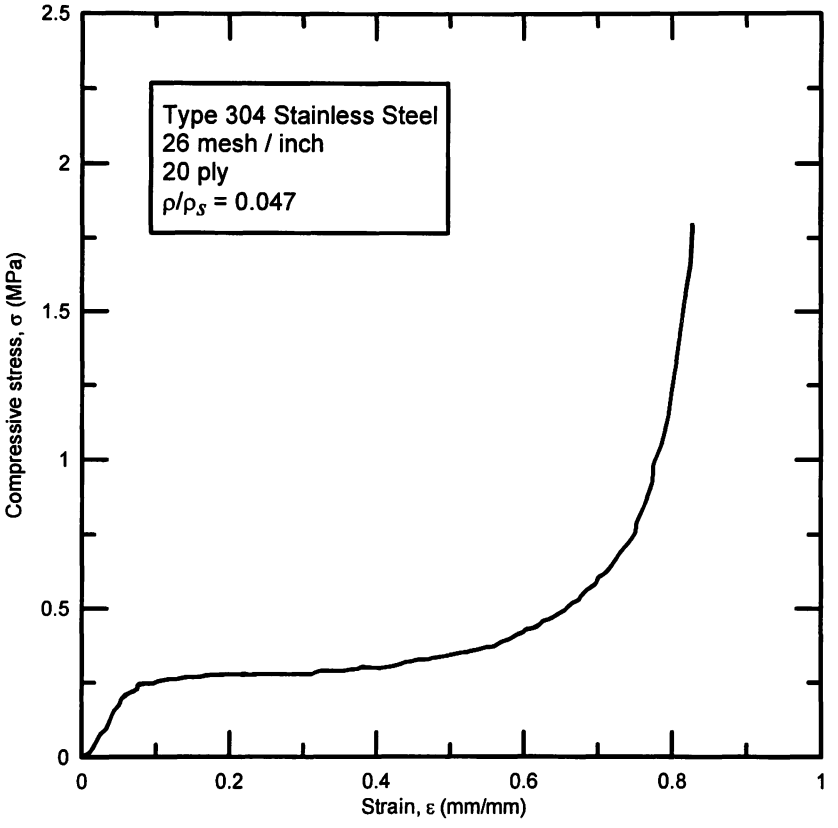

Figure 4-5. Stress-strain curve (sample C).

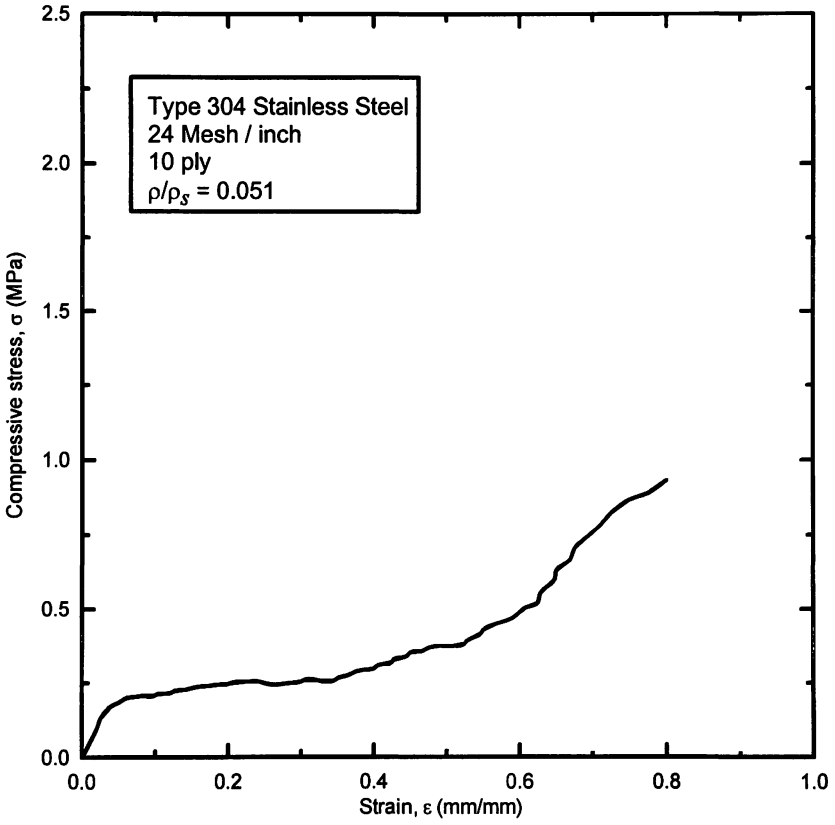

Figure 4-6. Stress-strain curve (sample A).

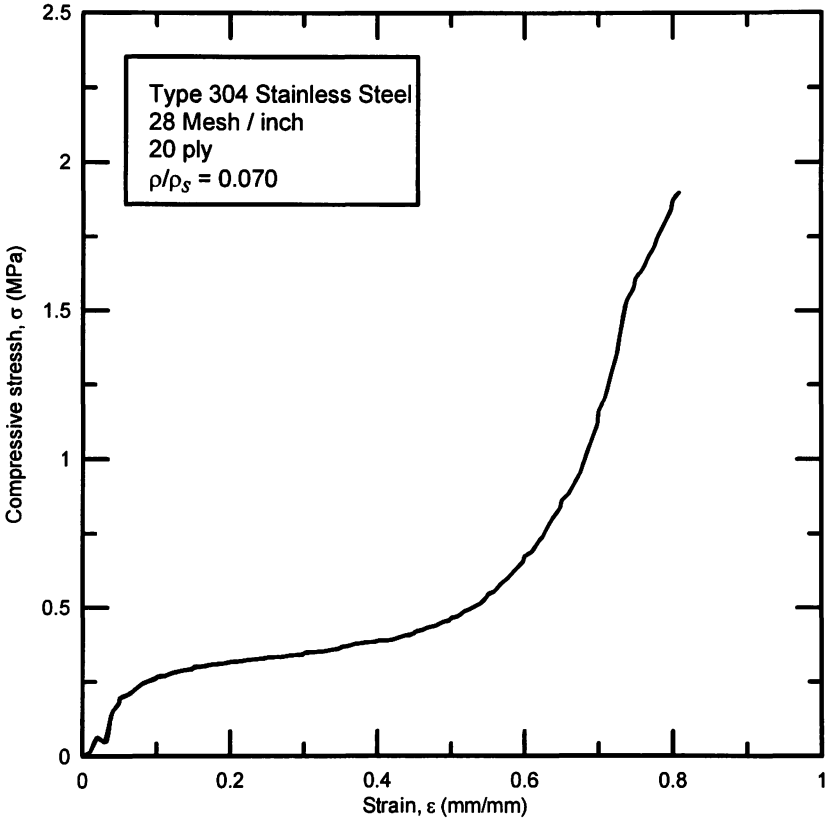

Figure 4-7. Stress-strain curve (sample D).

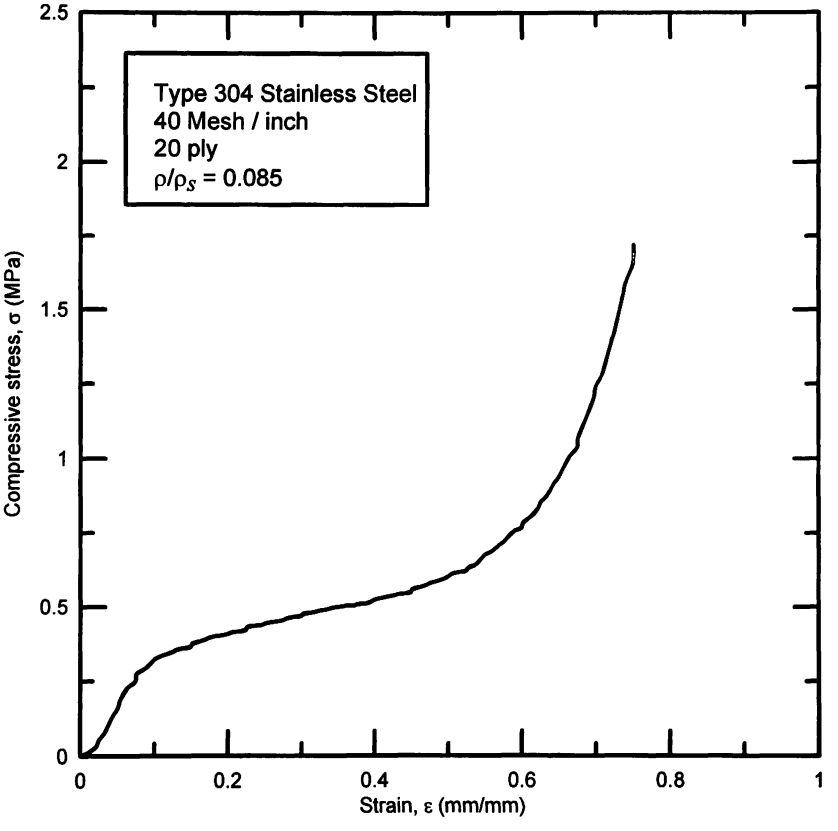

Figure 4-8. Stress-strain curve (sample F).

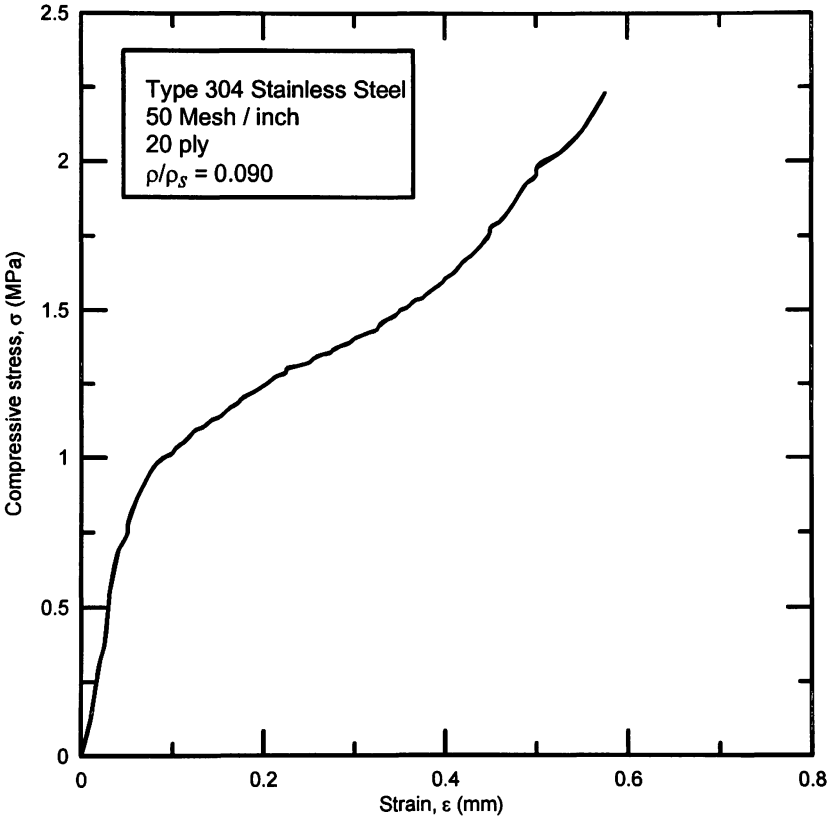

Figure 4-9. Stress-strain curve (sample G).

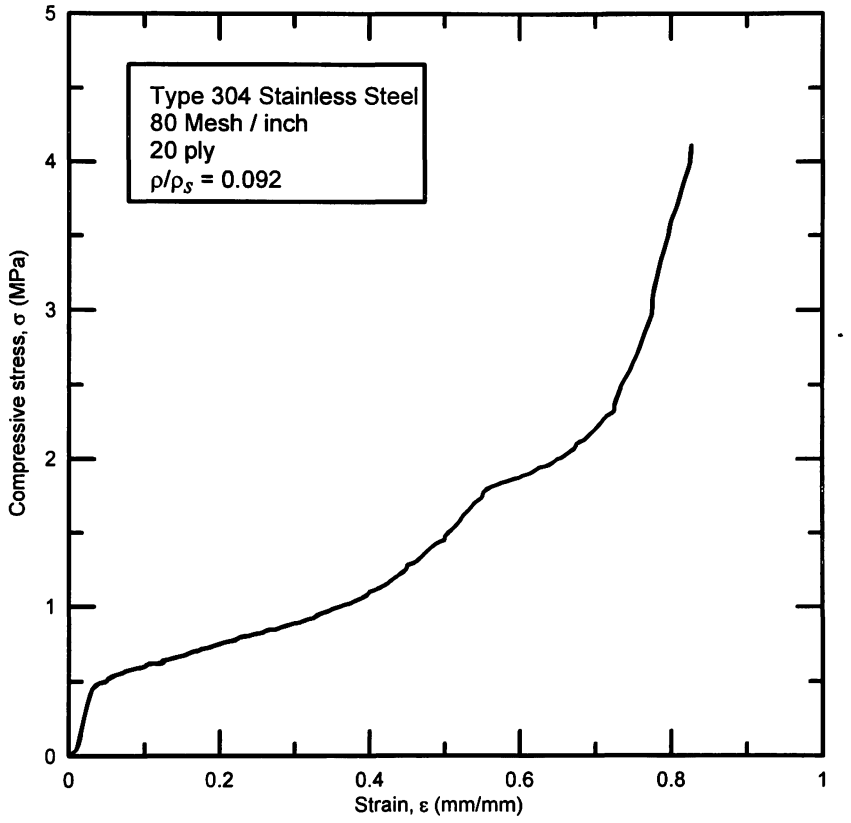

Figure 4-10. Stress-strain curve (sample H).

In Figs. 4-3 to 4-10, the plateau stress, $\sigma_{0.25}$, which is taken as the compressive yield strength at 25% strain for foams [43], was recorded. This plateau stress data will be used for comparison with model predictions. A tabulation of final sample test data is shown in Table 8.

Sample name	Stress $\sigma_{0.25}$ (MPa)	Strain (mm/mm)	ρ/ρ_s	$\sigma_{0.25}/\sigma_{ys}$
A	0.255	0.243	0.050	0.00124
B	0.273	0.258	0.045	0.00133
C	0.279	0.258	0.047	0.00136
D	0.253	0.250	0.068	0.00124
E	0.258	0.256	0.038	0.00126
F	0.449	0.257	0.084	0.00219
G	1.269	0.255	0.089	0.00619
H	0.825	0.255	0.091	0.00402

Table 8. Summary between relative density and relative compressive yield stress for the test samples.

4.3 Compressive Testing Discussion

The stress-stain curves shown in Figs. 4-3 to 4-10 indicate that wire diameter and opening width affect the final relative density of test samples, leading to differing relative compressive strengths. When performing compressive tests, interesting behavior was seen during the crushing motion. Tests were performed slowly in order to observe crushing of the individual layers. Crushing was not always initiated in the same location as the behavior was likely governed by defects. Bonds were occasionally heard breaking during the test as the ply collapsed. A plot of relative compressive stress as a function of relative density, Fig. 4-11, shows an increase in compressive yield strength with increasing relative density as anticipated.

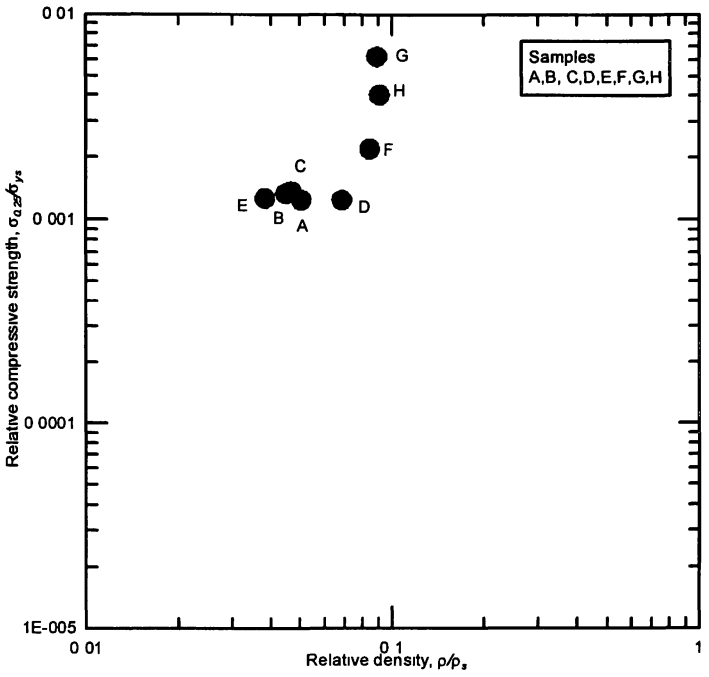

Figure 4-11. Comparison between relative density and relative compressive yield strength (samples: A, B, C, D, E, F, G, and H).

With Fig. 4-11, note that it is traditional to plot cellular solid data on a log-log scale owing to the large range of values and possibility for drawing straight lines fits through the data. Although samples G and H had nearly the same density and were made from the same base material, sample G was significantly stronger. It is believed that the higher strength for sample G is due the larger wire diameter and spacing as compared to Sample H which leads to better bonding between the corrugated layers.

4.4 Model Comparison

Figure 4-12 shows a comparison of relative compressive yield stress for tested samples (A, B, C, D, E, F, G, and H) and the Gibson-Ashby model for values of the constant C ranging from 0.1 to 0.5. A value of $C = 0.1$ or $C = 0.2$ appears to fit the test

data and with a similar slope as the model predictions. Thus, the corrugated samples based on type 304 stainless steel have compressive yield strengths that can be closely correlated to model predictions.

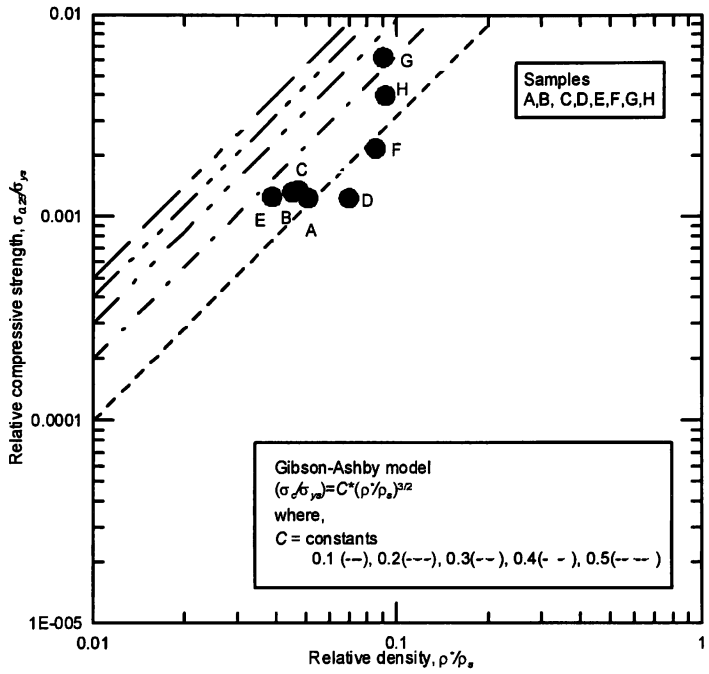

Figure 4-12. Comparison between compressive yield strength data and the Gibson-Ashby model.

5. DISCUSSION

5.1 Fabrication

It has been shown that cellular solids with open cells can be fabricated in a straightforward and economical way by corrugating inexpensive woven wire meshes and brazing them together in a controlled Ar atmosphere. A wide range of mesh size and wire diameter allowed substantial control over sample relative density and properties. By corrugating the wire mesh, the relative density as a 2-D cellular solid was substantially decreased through deformation in the out-of-plane direction. Then, by brazing the corrugated mesh together, 3-D cellular solids with interconnected open cells were created. The bonds were made using an Ag based brazing alloy in a heated Ar environment.

5.2 Performance

During compressive testing, the Ag based bonds were strong and tough enough to absorb large sample stresses during deformation without significant cracking. Wire diameter and opening width were found to significantly affect the final relative density of fabricated samples. By crimping, the relative density of the original uncrimped mesh was reduced by 70%-80%. During testing, it was observed that the relative density of fabricated samples has a significant effect on compressive yield strength. These strengths increased with increasing relative density and were found to be well correlated with the Gibson-Ashby open cell model.

5.3 Aerospace Applications

For aerospace applications, Ti alloys have been used for commercial jet parts such as airframes, bulkheads for a wide body, engine mounts, nacelle/pylon brackets, landing gear supporting structures, windshield frames, and flap carriages. For military jets, Ti alloys have been used for flap hinges for a wide body military transport jet. In addition, Ti alloys have been used for ordnance equipment, pressure vessels, rocket motors, and turbine parts such as blades, discs, wheels, and spacer ring cases [44]. However, very few cellular Ti alloys have been reported to date.

There are many Ti alloys used for aerospace and aircraft applications. For high strength, Ti-6Al-4V is often used. For creep and oxidation resistance in engines, Ti-6Al-2Sn-4Zr-2Mo (6-2-4-2), Ti-6Al-2Sn-4Zr-6Mo (6-2-4-6), and Ti-5.5Al-3.5Sn-3Zr-1Nb (829) are common [28]. Alloys of increasing importance for aircraft applications are Ti-6Al-2Zr-2Sn-2Mo-2Cr-0.25Si which is used for the airframe of the F-22 and JSF projects, and Ti-4.5Al-4Mo-4Sn-0.5Si (SP700) [28]. Less used titanium alloys in aircraft applications are Ti-4Al-4Mo-4Sn-0.5Si (551) for high strength airframes, and Ti-8Al-1Mo-1V for spares and replacements. Ti-11Sn-5Zr-2.5Al-1Mo-0.2Si (679) was an early engine alloy. Ti-6Al-5Zr-0.5Mo-0.2Si (685) was an engine alloy, and is now mainly for spares and replacements [28].

One can observe that Ti alloys have had a wide range of applications and uses in the aerospace industry. However, most Ti alloys for aerospace applications have not been made into cellular structures like open-cell or closed-cell foams. Thus, if fabricated into a cellular solid, potential new aerospace applications could arise. Few studies have reported this to date and the field is relatively wide open.

5.4 Biomedical Applications

Ti alloys have had a long successful history of use as implants within the human body [54]. Alloys used include 30% cold-worked Grade 4 Ti in conditions of forged, annealed, forged heat treatable, and so on [54]. These types of alloys are relatively inert within the human body, strong, stiff and light. They are normally used in their solid form when implanted. A few cellular forms of Ti alloys used within the body include flat woven meshes, bonded Ti spheres, etc. 3-D forms of the material with open cells have apparently not been reported to date. From the work in this thesis, it appears that open cell forms of Ti alloys could be made by a corrugation approach involving woven Ti meshes. These materials might then be used for biomedical applications such as hip replacement, artificial knee, and more. Being cellular, their properties would be a closer match to the natural structures they replace.

6. CONCLUSION

For many years, scientists and engineers have explored the fabrication and properties of new materials and structures. They have been trying to find or create materials with superior properties like those of cellular solids that are based on biological concepts. The study of cellular solids and structures made from them shows much potential for aerospace applications; especially lightweight structural materials that absorb impacts and blasts or provide for other functionalities owing to their interconnected porosity.

Here, these types of materials have been made from type 304 stainless steel with the focus on compressive yield strength over a range of relative density. During fabrication, three important results were achieved. First, it was shown that a wide range of mesh size and wire diameter can control the sample relative density. Second, by corrugating woven wire mesh, relative density was significantly decreased through deformation in the out-of-plane-direction. Third, economical 3-D cellular solids with open cells could be readily created by brazing the corrugated mesh together.

The stress-strain curves indicate that wire diameter and opening width affect the final relative density leading to differing relative compressive yield strengths. The corrugated samples based on type 304 stainless steel have compressive yield strengths that were closely correlated to the Gibson-Ashby open cell model predictions.

It is recommended that further research include investigation of linear elastic properties, optimization of cellular topology, finite element analysis of deformation

behavior, impact testing and energy absorption, as well as the use of titanium alloys for aerospace and biomedical applications.

REFERENCES

1. *The American Heritage Dictionary of the English Language* (4th editions, 2000). <http://www.bartleby.com/61/>
2. L. J. Gibson, M. F. Ashby (1997). *Cellular solids Structure and Properties,* 2nd ed., United Kingdom : Cambridge University Press, Cambridge.
3. A.Mark, S. Frans, (2004). *Solid-Liquid Interfaces: Molecular Structure, Thermodynamics, and Crystallization*, accesed December 10, 2004. <http://www.mrs.org/publications/bulletin>
4. J. Stampfl, R.Cano Vives, S. Seidler, R.Liska, F.Schwager, H.Gruber, A.Wob, P.Fratzl (Oct. 2003). *Rapid Prototype- A Route For The Fabrication of Biomimetic Cellular Materials*, the 1st International Conference on Advanced Research in Virtual and Rapid Prototyping, (Eds: P.J.Bartolo, G.Mitchell et al) 1.-4., Leiria, Portugal, pp 659-666.
5. Y. W. Kim, C. B. Park (2003). *Processing of microcellular preceramics using carbon dioxide,* Composites Science and Technology, 63, 2371-2377.
6. M. Brocca, P. Zdenek, Bazant, I. M. Daniel (2001). *Micro plane model for stiff foams and finite element analysis of sandwich failure by core indentation*, International Journal of Solids and Structures, 38, 8111-8132.
7. D. Matthew, Montminy, R. Allen, Tannenbaum, W. Christopher, Macosko (2004). *The 3D structure of real polymer foams*, Journal of Collide and Interface Science, 280, 202-211.
8. P. Rosakis, A. Ruina, R.S. Lakes, (1993). *Micro buckling instability in elastomeric cellular solids*, Journal of materials science, 28, 4667-4672.
9. H. Sakamoto, K. Ishimura, M.C. Natori, K. Higuchi (2000). *Concepts of Redundant Space Structures Using Multi-Cellular Inflatable Elements,* Eleventh international conference on adaptive structures and technologies, Oct 23-26.
10. H.S. Kim, S.T.S. Al-Hassani (2002). *A morphological model of vertebral trabecular bone,* Journal of Biomechanics, 35, 1101-1114.
11. L.L. Hench, J.M. Polak (8 February 2002). *Third-Generation Biomedical Materials*, SCIENCE, Vol. 295, 1014-1017.
12. N. Harlan (September 2000). *Titanium Bone Implants*, Materials Technology, Vol. 15, No. 3, pp. 185-187.
13. N. Harlan, R. Reyes, D.L. Bourell (August 2000). *Building Better* Bones, Foundry Management & Technology, Vol.128, No. 8, pp.82-83.
14. B.D. Ratner and A.S. Hoffman, F.J. Schoen, J.E. Lemons (1996). *Biomaterials Science- An Introduction to Materials in Medicine,* Academic Press, Elsevier Science (USA).

15. J.A.Elliott, A.H.Windle, J.R.Hobdell, G.Eeckhaut, R.J.Oldman, W.Ludwig, E.Boller, P.Cloetens, J.Baruchel (2002). *In-situ deformation of opened-cell flexible polyurethane foam characterized by 3D computed micro tomography,* Journal of materials science; 37:1547-1555.

16. M.Warner, B.L. Thiel, and A.M.Donald (2000). *The elasticity and failure of fluid-filled cellular solids Theory and experiments,* PNAS, February 15, Vol. 97, No. 4, 1370-1375.

17. P. E. Arzt. *Metal-matrix composites cellular materials and mechanical spectroscopy,* department Arzt-research areas, accessed December 13, 2004. <http://finix.mpistuttgart.mpg.de/arzt/mf_mpg_abteilungen_e/mf_mpg_abteilungen_arzt/composites.html>

18. E. Wu (1995). *Plastic Buckling of Metallic Honeycombs,* Journal of the Chinese Society of Mechanical Engineers, Vol. 16, No. 1, pp.11~20.

19. V.S. Deshpande, N.A. Fleck, M.F. Ashby (2001). *Effective properties of the octet-truss lattice material,* Journal of Mechanics and Physics of Solids, 49, 1747-1769.

20. Erik S. Weiser and Brian W. Grimsley, R. Byron Pipes, Martha K. Williams (2002). *Polyimide foams from friable balloons,* accessed May 20, 2004. <http://techreports.larc.nasa.gov/ltrs/PDF/2002/mtg/NASA-2002-47sampe-esw.pdf>

21. R. Lakes (1996). *Cellular solid structures with unbounded thermal expansion,* Journal of materials science letters, 15, 475-47.

22. S. Lee, F. Barthelat, H.D. Espinosa (2003). *Strain Rate Effects In Metallic Cellular Materials,* 2003 SEM Annual Conference and Exposition on Experimental and Applied Mechanics, June 2-4, Charlotte, North Carolina,Session 37, Paper 188.

23. R.E. Crowe, F. Daniel, S. Marin (August 1995). *The protection and rehabilitation of dams using cellular confinement systems*, accessed May 25, 2005. <http://www.prestogeo.com/files/pdfs/dam_rehabilitation.pdf>

24. P. Colombo, J.R. Hellmann, D.L. Shelleman (2001). *Mechanical properties of silicon ox carbide ceramic foams*, J.Am.Ceram.Soc., 84 [10] 2245-51.

25. V.S. Deshpande, N.A. Fleck (2000). *High strain rate compressive behavior of aluminum alloy foams,* International Journal of Impact Engineering, 24, 277-298.

26. J. Tian, T. Kim, T. J. Lu, H. P. Hodson, D. T. Queheillalt, D. J. Sypeck, H. N. G. Wadley (2004). *The effect of topology upon fluid-flow and heat-transfer within cellular copper structures*, International Journal of Heat and Mass Transfer, 47, 3171-3186.

27. Z. Song, L. Ma, Z. Wu, D. He (2000). *Effects of viscosity on cellular structure of foamed aluminum in foaming process*, Journal of Materials Science, 35, 15-20.

28. AZoM.com Ptv., Ltd, *Titanium alloys for aeroengine and airframe applications*, accessed May 30, 2004. <http://www.azom.com/detai;s.asp?/ArticleID=1569>

29. Oliveira, C. Prud'homme, K. Veroy, A.T. Patera, *Thermo-structural analysis of multifunctional prismatic cellular(triangular) metals,* Department of Mechanical Engineering,

30. Z. Fang, B. Starly, W. Sun (2005). *Computer-aided characterization for effective mechanical properties of porous tissue scaffolds,* Computer-Aided Design, 37, 65-72.

31. S. Kishimoto, N. Shinya (1998). *Development of Metallic Closed Cellular Materials Containing Polymers*, Materials in space-science, technology, and exploration: Symposium held November 29 – December 2, 1998, Boston, Massachusetts, U.S.A., 291-296.

32. A.P.Roberts, E.J.Garboczi (2001). *Elastic Module of Model Random three-Dimensional Closed Cellular Solids,* National Institute of Standards and Technology, 2001 Acta Materialia, Vol. 49, No.2, 189-197.

33. R.Pippan, C. Motz (2004). *Metallic foams*, accessed June •5, 2004. <http://www.oeaw.ac.at/esi/english/research/materials/cell/met-foam.html>

34. S.P. Timoshenko, J.N. Goodier (1934, c1970). *Theory of elasticity.* 3rd ed, New York, GcGraw-Hill.

35. Pytel, F.L.Singer (1987). *Strength of Materials*, 4th edition, Harper Collins Publishers Inc.

36. D.J. Sypeck, H.N.G. Wadley (March 2001). *Multifunctional microtruss laminates: Textile synthesis and properties*, J. Mater. Res, Vol. 16, No. 3, pp 890–897.

37. N.G. Haydn, Wadley, A. Norman, Fleck, G. Anthony, Evans (2003). *Fabrication and structural performance of periodic cellular metal sandwich structures*, Composites Science and Technology 63,pp 2331-2343.

38. D.J. Sypeck, H.N.G. Wadley (2002). *Advanced Engineering Materials,* 4, No.10.

39. G. Petzow (January 2001). *Metallographic Etching*, 2nd Edition, ASM International Information Society, pp142.

40. Cleveland wire cloth Ltd. Accessed June 7, 2004. <http://www.wirecloth.com/titanium.htm>

41. McMaster-Carr Supply Company. Accessed June 7, 2004. <http://www.mcmaster.com>

42. Lucas-Milhaupt, Inc., *VTG/High purity silver, gold, palladium*, accessed May 20, 2004.<http://www.lucasmilhaupt.com/htmdocs/brazing_products/brazing_filler_metals/high_purity.html>

43. Granta Material Intelligence Inc., *Materials for bicycle helmets*, accessed July 5, 2004. <http://www.grantadesign.com/resources/materials/casestudies/helmet.htm>

44. K. Boomsma (March 2002). *The effects of compression and pore size variations on the liquid flow characteristics in metal foams*, Journal of Fluids Engineering,

Vol. 124, 263-272.

45. A.E. Simon, L.J. Gibson (1998). *Acta Mat.*, **46**, 2139.

46. Bo'sun supplies, Co., *Stainless steel info.*, accessed July 13, 2004. <http://bosunsupplies.com/StainlessInfo2.cfm>

47. A.M. Helmenstine, *Why is Stainless Steel Stainless?*, accessed July 13, 2004. <http://chemistry.about.com/cs/metalsandalloys/a/aa071201a.htm>

48. D. Buddy, Ratner, S. Allan, Hoffman, J. Frederick, Schoen, E. Jack, Lemons (1996). *An Introduction to Materials in Medicine,* Academic press, Biomaterials Science, pp43-50.